

# Superfluidity and Quantum Geometry in Twisted Multilayer Systems

Päivi Törmä,<sup>1,\*</sup> Sebastiano Peotta,<sup>1</sup> and Bogdan A. Bernevig<sup>2,3,4</sup>

<sup>1</sup>*Department of Applied Physics, Aalto University School of Science, FI-00076 Aalto, Finland*

<sup>2</sup>*Department of Physics, Princeton University, USA*

<sup>3</sup>*Donostia International Physics Center, P. Manuel de Lardizabal 4, 20018 Donostia-San Sebastian, Spain*

<sup>4</sup>*IKERBASQUE, Basque Foundation for Science, Bilbao, Spain*

Designer 2D materials where the constituent layers are not aligned may result in band structures with dispersionless, “flat” bands. Twisted bilayer graphene has been found to show correlated phases as well as superconductivity related to such flat bands. In parallel, theory work has discovered that superconductivity and superfluidity is determined by the quantum geometry and topology of the band structure. These recent key developments are merging to a flourishing research topic: understanding the possible connection and ramifications of quantum geometry on the induced superconductivity and superfluidity in moiré multilayer and other flat band systems. This article presents an introduction to how quantum geometry governs superfluidity in platforms including, and beyond, graphene. We explain how a new type of topology discovered in TBG could affect superconductivity, pinpoint the geometric contribution in its Beretinskii-Kosterlitz-Thouless (BKT) critical temperature, and mention moiré materials beyond TBG. Ultracold gases are introduced as a complementary platform for quantum geometric effects and a comparison is made to moiré materials. An outlook sketches the prospects of twisted multilayer systems in providing the route to room temperature superconductivity.

## I. INTRODUCTION

Superconductivity or superfluidity require bosonic particles to be in the same energy state; in case of superconductors these bosons are composites of two electrons, so-called Cooper pairs. However, being in the same state is not alone sufficient. The system needs to be able to host stable supercurrents, that is, dissipationless flow of particles: this is what makes superconductors useful in generating large magnetic fields or in providing qubits for quantum computing. It has long been the holy grail of condensed matter physics to bring the phenomenon of superconductivity to room temperature, and research on high- $T_c$  materials has been leading the way [1]. However, a complementary route is now emerging, that of purposefully designing materials less complex, and more tunable, than the traditional high- $T_c$  ones, following simple but fundamental theory guidelines.

The first theory guideline for achieving high temperature superconductivity is to use bands where the energy dispersion as function of momentum,  $\varepsilon(\mathbf{k})$ , is constant – so-called flat bands. The critical temperature  $T_c$ , at which Cooper pairs form, is predicted [2–4] to be linearly proportional to the interaction  $U$  between the Cooper pair constituents. Comparison to the well-known prediction of the Bardeen-Cooper-Schrieffer (BCS) theory of superconductivity [5],  $T_c \propto e^{-1/(n_F U)}$  ( $n_F$  is the density of states at the Fermi level) shows that the critical temperature is *exponentially enhanced* compared to dispersive systems, in the BCS formalism. The band does not need to be exactly flat to benefit from this; any band where the interaction  $U$  is much larger than the bandwidth will do.

A second guideline from theory, however, is needed since the flat band provides only the critical temperature

for Cooper-pairing but does not determine whether superfluidity and supercurrents exist. Their existence is not obvious in a flat band: if non-interacting fermionic particles are localized on atomic sites and their ground state is an insulator, then no current is possible. Would interacting particles as well just form localized pairs which cannot move? Or, is supercurrent possible, and if yes, under which general conditions? The answer was found only relatively recently: stable supercurrent and superfluidity are possible even in a flat band, if the band has non-trivial *quantum geometry* [6–9]. The quantum geometry here refers to distances and curvatures in the space (or manifold) formed by the electronic Bloch functions, i.e. the eigenfunctions of the band.

The quantum geometry of a band is characterized by the quantum geometric tensor [10, 11]. Its real part is the quantum metric, which quantifies the amplitude distance between two close quantum states. Quantum states have, however, also a phase difference, leading to the definition of the Berry phase. Indeed, the imaginary part of the quantum geometric tensor is the Berry curvature. Integrated over the Brillouin zone, the Berry curvature gives the Chern number – an integer – a topological invariant that changes only stepwise. Non-zero values of the quantum metric or of the Berry curvature make the quantum geometry of the system non-trivial. If the Chern number is non-zero, the system is also topologically non-trivial. These concepts are defined in Box 1. The Berry curvature is known to be relevant for numerous physical phenomena, including topological insulators and superconductors [12, 13], while the importance of the quantum metric is only emerging – it turns out to be the quantity that governs flat band superconductivity.

The underlying reason why quantum geometry is important for superconductivity and superfluidity is that it determines the *overlaps between the eigenstates* in a band. If the wavefunctions are exponentially localized at

\* [paivi.torma@aalto.fi](mailto:paivi.torma@aalto.fi)

the lattice sites, or delta-function localized in the atomic limit, the overlaps vanish; this is a trivial flat band. However, there are many systems where flat bands occur in conjunction with mobile – not atomic – electrons. Many lattice geometries, such as – but not limited to – the Lieb lattice, support eigenstates with opposite phases at nearby lattice sites, so that tunneling contributions from neighboring sites interfere destructively. This leads to a set of degenerate eigenstates, i.e. a flat band. Another route to nearly flat bands are superlattices that introduce new, smaller Brillouin zones (BZ), and consequently new band gaps that then lead to band flattening; see Fig. 1 upper panel. Band gap opening is given, in general, by the interference between a state of certain momentum and a backscattered state with opposite momentum. Therefore both mechanisms of flat band generation rely on the quantum interference of the wave functions. One is best illustrated in the real space and the other in the momentum space. Many types of lattices (line-graph lattices, split graph, Lieb, etc. [14–16]) can support flat bands which result from wavefunction interference. A large number of such-obtained flat bands are topological in origin [17] and exhibit nonzero (non-Abelian) Berry curvature. Whether or not adding interaction to these bands leads to transport and supercurrent depends on the overlap of the Wannier functions, that is, the Fourier transforms of the Bloch functions, see Fig. 1 lower panel. The overlap, in turn, is governed by quantum geometry. This explains the quantum geometric origin of flat band superconductivity.

In the quest for room temperature superconductivity, one thus needs to design not only the band dispersion but also the properties of the Bloch functions, that is, the band geometry and topology. Twisted bilayer graphene (TBG) and other moiré materials, where a superlattice is created by a twist angle between two graphene layers, offer unprecedented potential for flat band engineering and control [18–22]. At about one degree, so-called first magic angle, a set of flat bands appears in the electronic spectrum. The individual graphene sheets have finite Berry curvatures near the four Dirac points of TBG (two per layer, located at the  $K$  and  $K'$  high-symmetry points of the BZ called valleys). Inter-layer hopping of electrons *couples* the Dirac points of the *same* valley and Berry curvature (also called here "helicity") in the two layers. In contrast, the *different* valleys are *decoupled*. The coupling of the same valley, same helicity Dirac nodes, with their additive helicity, leads to the emergence of a new type of topology of the single-valley model of TBG. Further degrees of freedom in the design of bands and their topology are given by stacking more than two graphene layers, or creating moiré materials composed of other elements than carbon. Quantum gases of ultracold atoms form another playground for the study of interacting flat bands. In these systems, one can create moiré geometries as well as simpler flat band systems such as Lieb and kagome lattices, and tune the interparticle interaction over a wide range from repulsive to attractive using Feshbach reso-

nance techniques.

In this review, we first introduce the essential theory of quantum geometry-dependence of superfluidity, and show how a finite Chern number of a band gives a fundamental lower bound of the flat band superfluid weight, the observable that quantifies the ability of the system to support superfluid transport. We then explain how a similar lower bound is given by a new type of zero-Chern-number topology in the context of TBG, and review theory work that predicts the relevance of quantum geometric effects in the experimentally observed TBG superconductivity and other materials. We then review the work on moiré systems in ultracold gases. We discuss the prospects of reaching room temperature superconductivity by band structure and topology design, and briefly refer to the exciting possibilities available for bosonic condensates of atoms, polaritons or photons in flat bands.

## II. THE QUANTUM GEOMETRIC CONTRIBUTION OF SUPERFLUID WEIGHT: TOPOLOGICAL LOWER BOUND FOR SUPERCURRENT

### A. Superfluid weight

The electrodynamic properties of superconducting materials are captured by the constitutive relation (in London gauge) [5, 23]

$$\mathbf{j} = -D_s \mathbf{A}, \quad (7)$$

with  $\mathbf{j}$  the current density and  $\mathbf{A}$  the vector potential. In tandem with Maxwell's equations, Eq. (7) provides a quantitative description of the phenomena of perfect conductivity and perfect diamagnetism (Meissner effect), therefore a nonzero superfluid weight  $D_s \neq 0$  is the very criterion of superconductivity [24, 25]. The superfluid weight measures also the energy required to create a modulation of the phase  $\phi(\mathbf{r})$  of the superconducting order parameter  $\psi(\mathbf{r}) = |\psi(\mathbf{r})|e^{i\phi(\mathbf{r})}$  since the free energy contains the term

$$\Delta F = \frac{\hbar^2}{2e^2} \int d^d \mathbf{r} \sum_{ij} D_{s,ij} \partial_i \phi(\mathbf{r}) \partial_j \phi(\mathbf{r}), \quad (8)$$

with  $d = 2, 3$  the spatial dimension,  $\hbar$  the Planck's constant and  $e$  the electron charge. In anisotropic systems the superfluid weight is not a scalar but a rank-2 tensor  $D_{s,ij}$  and Eq. (7) is modified accordingly.

The standard result for the superfluid weight of a spinful electron band at zero temperature given by BCS theory is [5, 26]

$$D_{s,ij} = \frac{e^2}{\hbar^2} \int \frac{d^d \mathbf{k}}{(2\pi)^d} f(\varepsilon(\mathbf{k})) \frac{\partial^2 \varepsilon(\mathbf{k})}{\partial k_i \partial k_j}. \quad (9)$$

where  $\varepsilon(\mathbf{k})$  is the dispersion of the band. Here and in the following, quasimomentum  $\mathbf{k}$  integrals are performed over the first BZ. The function  $f(\varepsilon)$  is the occupation of a single-particle state with energy  $\varepsilon$  in the

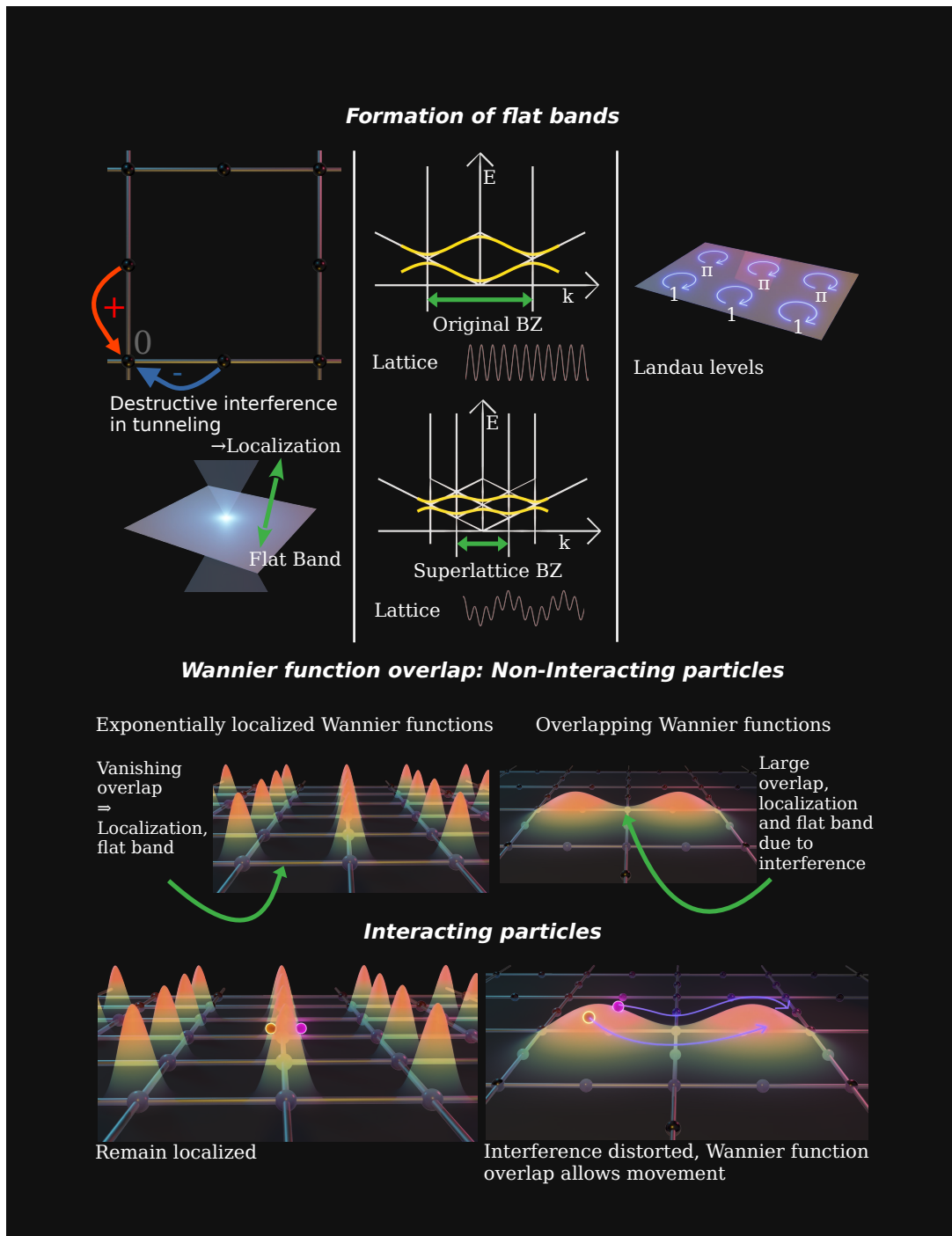


Figure 1. **Formation of flat bands and the role of Wannier function overlap in flat band superfluidity.** Upper panel: (left) Certain lattice geometries, such as the Lieb lattice example, support eigenstates that occupy a subset of lattice sites with such phases of the wavefunction that tunneling to the rest of the sites is impossible due to destructive interference, leading to localized states and a flat band. (middle) Introducing a superlattice on top of a periodic system, a BZ smaller than the original emerges, and if new band gaps are opened, band flattening takes place. (right) Landau levels are a well-known example of a flat band system. One can understand the localization and band flattening via plaquettes with winding phases so that interference prevents movement, or alternatively, one may think the plaquettes as forming a larger unit cell and a superlattice. Lower panels: Non-interacting particles can be immobile either if their Wannier functions are exponentially localized at the lattice sites, or due to destructive interference. In the former case, also interacting particles will be localized, while in the latter, interactions distort the interference and the particles can move due to the finite overlap of the Wannier functions. Wannier function overlaps are controlled by the quantum geometry of the band; in particular, topological systems cannot have exponentially localized Wannier functions. Picture by Antti Paraoanu. The style of the figure is not final.

BCS ground state [5, 23]. By assuming an approximately parabolic band  $\varepsilon(\mathbf{k}) \approx \hbar^2 \mathbf{k}^2 / (2m_{\text{eff}})$  in Eq. (9), one obtains  $D_s = e^2 n / m_{\text{eff}}$ , where  $n$  is the total number density and  $m_{\text{eff}}$  the particle effective mass [27]. At finite temperature only a fraction of the charge carriers participate to superfluid transport, thus the superfluid weight reads  $D_s = e^2 n_s / m_{\text{eff}}$  where  $n_s$  is the superfluid density and  $0 \leq n_s / n \leq 1$  the corresponding superfluid fraction [5, 23, 28]. In the extreme limit in which the single-particle effective mass is very large or even diverging, the superfluid weight should be very small or even vanishing according to Eq. (9) [29]. To best understand why this is not generally the case in multiband systems, it is illuminating to first consider the two-body problem in a flat band [9].

### B. Geometric origin of the pair effective mass in a flat band

Leon Cooper showed that the Fermi sea is unstable towards pair formation under an arbitrarily small attractive interaction between electrons [5], even when in three dimensions the strength of a short-range attractive interaction needs to be larger than a threshold for two quantum particles to form a bound state. In the limit of infinite effective mass, that is in a flat band, a bound state is always present for any small value of the attractive interaction strength [9]. A crucial question is: what is the effective mass of the bound state? Naively, one could expect that since the constituent particles have infinite effective mass this would be the case also for the bound state they form. This would mean that the superfluid weight is zero and no superconducting state can occur in a partially filled flat band. However, one can show that the bound state can disperse as a result of interactions. An estimate of the dispersion of the two-body bound state is obtained as [9]

$$\begin{aligned} E(\mathbf{q}) &= -U\Omega_c \int \frac{d^d \mathbf{k}}{(2\pi)^d} \sum_{\alpha=1}^{N_{\text{orb}}} P_{\alpha\alpha}(\mathbf{k}) P_{\alpha\alpha}(\mathbf{k} - \mathbf{q}) \\ &= -U\Omega_c \int \frac{d^d \mathbf{k}}{(2\pi)^d} \sum_{\alpha=1}^{N_{\text{orb}}} |u_{\bar{n}\mathbf{k}}(\alpha) u_{\bar{n}\mathbf{k}-\mathbf{q}}(\alpha)|^2. \end{aligned} \quad (10)$$

Here  $\Omega_c$  is the unit cell volume,  $N_{\text{orb}}$  the number of orbitals per unit cell,  $u_{\bar{n}\mathbf{k}}(\alpha)$  are the periodic Bloch functions of the  $\bar{n}$ -th band, which is flat, and  $P_{\alpha\beta}(\mathbf{k}) = u_{\bar{n}\mathbf{k}}(\alpha) u_{\bar{n}\mathbf{k}}^*(\beta)$  are the matrix elements of the corresponding band projector  $P(\mathbf{k})$ , an  $N_{\text{orb}} \times N_{\text{orb}}$  matrix. This result holds in the case of spin-1/2 fermions moving in a lattice and interacting by means of an attractive Hubbard interaction of the form  $\hat{H}_{\text{int}} = -U \sum_{\mathbf{i}\alpha} \hat{n}_{\mathbf{i}\alpha\uparrow} \hat{n}_{\mathbf{i}\alpha\downarrow}$  ( $U > 0$ ), where  $\hat{n}_{\mathbf{i}\alpha\sigma} = \hat{c}_{\mathbf{i}\alpha\sigma}^\dagger \hat{c}_{\mathbf{i}\alpha\sigma}$  is the occupation number operator of the lattice site labelled by the unit cell index  $\mathbf{i} = (i_1, i_2, i_3)$ , and the sublattice (orbital) index  $\alpha$ , while  $\sigma = \uparrow, \downarrow$  is the spin index. Time-reversal

symmetry has also been assumed, as a consequence  $u_{\bar{n}\mathbf{k}}(\alpha) = u_{\bar{n}\mathbf{k}\uparrow}(\alpha) = u_{\bar{n}, -\mathbf{k}, \downarrow}^*(\alpha)$ .

Due to the time-reversal symmetry, the point  $\mathbf{q} = \mathbf{0}$  in the Brillouin zone is an extremum of the dispersion. Then from Eq. (10), we obtain an estimate for the effective mass tensor of the bound state [9]

$$\begin{aligned} \left[ \frac{1}{m_{\text{eff}}} \right]_{ij} &\approx \frac{U\Omega_c}{\hbar^2} \int \frac{d^d \mathbf{k}}{(2\pi)^d} \sum_{\alpha=1}^{N_{\text{orb}}} \partial_i P_{\alpha\alpha}(\mathbf{k}) \partial_j P_{\alpha\alpha}(\mathbf{k}) \\ &\approx \frac{U\Omega_c}{N_{\text{orb}} \hbar^2} \int \frac{d^d \mathbf{k}}{(2\pi)^d} \text{Tr} [\partial_i P(\mathbf{k}) \partial_j P(\mathbf{k})] \\ &= \frac{U\Omega_c}{N_{\text{orb}} \hbar^2} \int \frac{d^d \mathbf{k}}{(2\pi)^d} g_{jl}(\mathbf{k}). \end{aligned} \quad (11)$$

We used the approximation  $\sum_{\alpha=1}^{N_{\text{orb}}} \partial_i P_{\alpha\alpha}(\mathbf{k}) \partial_j P_{\alpha\alpha}(\mathbf{k}) \approx N_{\text{orb}}^{-1} \sum_{\alpha, \beta=1}^{N_{\text{orb}}} \partial_i P_{\alpha\beta}(\mathbf{k}) \partial_j P_{\beta\alpha}(\mathbf{k})$  to obtain the second line [9]. The quantity  $g_{jl}(\mathbf{k})$  is the quantum metric (see Box 1). Eq. (11) teaches us that the effective mass of a two-body state in a flat band depends both on the interaction strength and on the quantum metric, which is purely a property of the single-particle wavefunctions.

The analysis of the two-body problem shows that Cooper pairs can have a finite effective mass and thus support transport if the flat band has a nonzero quantum metric. This is in sharp contrast with Eq. (9), which gives a zero result for the superfluid weight of a partially filled single (or non-hybridizing) flat band, showing that Eq. (9) neglects additional contributions that come into play in the case of multiband/multiorbital lattices ( $N_{\text{orb}} > 1$ ). These can be obtained from standard BCS theory applied to multiband lattice models. They were identified only recently [6–8] and we give a brief account of these results using a linear response theory approach [8].

### C. Conventional and geometric contributions of the superfluid weight

The vector potential  $\mathbf{A}(\mathbf{r}, t)$  enters in the non-interacting part of the Hamiltonian through the Peierls phases  $\phi_{\mathbf{i}\alpha, \mathbf{j}\beta}(t)$

$$\hat{H}_{\text{free}} = \sum_{\mathbf{i}\alpha, \mathbf{j}\beta} \hat{c}_{\mathbf{i}\alpha}^\dagger K_{\mathbf{i}\alpha, \mathbf{j}\beta} e^{i\phi_{\mathbf{i}\alpha, \mathbf{j}\beta}(t)} \hat{c}_{\mathbf{j}\beta}, \quad (12)$$

$$\phi_{\mathbf{i}\alpha, \mathbf{j}\beta}(t) = \frac{e}{\hbar} \int_{\mathbf{r}_{\mathbf{j}\beta}}^{\mathbf{r}_{\mathbf{i}\alpha}} d\mathbf{r} \cdot \mathbf{A}(\mathbf{r}, t). \quad (13)$$

The matrix  $K_{\mathbf{i}\alpha, \mathbf{j}\beta}$  contains the hopping amplitudes between the lattice sites and the on-site potential. The spin index has been absorbed in the orbital index ( $\alpha\sigma \rightarrow \alpha$ ). Expanding the non-interacting Hamiltonian in powers of the vector potential as  $\hat{H}_{\text{free}} = \hat{H}_0 + \hat{H}_1 + \dots$  gives, for the first order term,  $\hat{H}_1 = -V \sum_{\mathbf{q}} \mathbf{A}(\mathbf{q}, t) \cdot \hat{\mathbf{J}}(-\mathbf{q})$ , where  $V$  is the volume in  $d = 3$ ,  $\mathbf{A}(\mathbf{q}, t) = V^{-1} \int d^d \mathbf{r} \mathbf{A}(\mathbf{r}, t) e^{-i\mathbf{q} \cdot \mathbf{r}}$  and  $\hat{\mathbf{J}}(\mathbf{q})$  are the Fourier transforms of the vector potential and of the current density, respectively. The superfluid



### Box 1: Band structure invariants and topology

The eigenfunctions of a Bloch band, describing electrons in crystalline materials, are the periodic Bloch functions  $|u_{n\mathbf{k}}\rangle$ , where  $n$  denotes the band number. They are defined up to a  $\mathbf{k}$ -dependent phase, and can enter the expression of an observable quantity only through band structure invariants, which do not depend on how this phase is chosen (sometimes called a gauge choice).

A basic invariant is the **quantum geometric tensor (QGT)**

$$\mathcal{B}_{ij}(\mathbf{k}) = 2\text{Tr}[P(\mathbf{k})\partial_i P(\mathbf{k})\partial_j P(\mathbf{k})]. \quad (1)$$

It is expressed in terms of the projector to the band  $n$  of interest,  $P(\mathbf{k}) = |u_{n\mathbf{k}}\rangle\langle u_{n\mathbf{k}}|$ , which is unchanged under the gauge transformation  $|u_{n\mathbf{k}}\rangle \rightarrow e^{i\theta(\mathbf{k})}|u_{n\mathbf{k}}\rangle$ . Importantly, the QGT is a Hermitian matrix with non-negative eigenvalues, i.e. a positive semi-definite complex matrix.

Using the property  $P(\mathbf{k}) = P^\dagger(\mathbf{k}) = P^2(\mathbf{k})$ , the real part of the QGT can be written as

$$g_{ij}(\mathbf{k}) = \text{Re } \mathcal{B}_{ij}(\mathbf{k}) = \text{Tr}[\partial_i P(\mathbf{k})\partial_j P(\mathbf{k})] \quad (2)$$

and is known as the **quantum metric** (or Fubini-Study metric). It is a measure of the distance between infinitesimally close wave functions in  $\mathbf{k}$ -space. The quantum metric appears also as the gauge-invariant part of the Marzari-Vanderbilt localization functional for Wannier functions (see Sec. II D).

The imaginary part of the QGT is related to the concept of Berry (geometric) phase. Let us first remind about the Berry connection in band  $n$

$$\mathbf{A}(\mathbf{k}) = i \langle u_{n\mathbf{k}} | \nabla_{\mathbf{k}} u_{n\mathbf{k}} \rangle. \quad (3)$$

The Berry phase can be expressed as an integral over a surface  $S$  whose boundary is a closed curve  $\gamma = \partial S$

$$\Phi_{\text{Berry}} = \int_S d\mathbf{S} \cdot \nabla_{\mathbf{k}} \times \mathbf{A}(\mathbf{k}) = \frac{1}{2} \int_S dS_l \varepsilon^{lmn} \text{Im } \mathcal{B}_{nm}(\mathbf{k}). \quad (4)$$

The quantity  $\nabla_{\mathbf{k}} \times \mathbf{A}(\mathbf{k})$ , proportional to the imaginary part of the QGT, is known as the **Berry curvature**. If in the above equation the integral is extended to the whole Brillouin zone (assuming dimension  $d = 2$ ) one obtains the so-called **Chern number**, a topological invariant,

$$\mathcal{C} = \frac{1}{2\pi} \int_{\text{BZ}} d^2\mathbf{k} \text{Im } \mathcal{B}_{12}(\mathbf{k}). \quad (5)$$

The Chern number can take only integer values.

The fact that the QGT is positive semi-definite implies that the real and imaginary parts satisfy a number of constraints, of which Eq. (24) is an example. The Berry connection  $\mathbf{A}(\mathbf{k})$  and curvature can be generalized to the case of multiple bands ( $\mathbf{A}^{mn}(\mathbf{k}) = i \langle u_{m\mathbf{k}} | \nabla_{\mathbf{k}} u_{n\mathbf{k}} \rangle$ ), in which case they are called non-Abelian and bring about a wide array of new topological invariants. One example is the **Euler class**,  $e_2$ , is a topological invariant expressed in terms of the non-Abelian Berry curvature. In systems with  $C_{2z}T$  symmetry, the non-Abelian Berry connection and curvature of two bands can be written as  $\mathbf{A}(\mathbf{k}) = -\mathbf{a}(\mathbf{k})\sigma_y$  and  $\mathcal{F}_{xy}(\mathbf{k}) = -f_{xy}(\mathbf{k})\sigma_y$ , respectively ( $\sigma_y$  is a Pauli matrix). The Euler class  $e_2$  is the invariant defined as

$$e_2 = \frac{1}{2\pi} \int d^2k f_{xy}. \quad (6)$$

The abelian QGT in Eq. (1) is the trace of a more general, positive-definite **non-Abelian QGT** (matrix)  $\mathfrak{G}_{ij}$ : if the Bloch states for  $n = 1 \dots N$  bands are written as a vector  $u(\mathbf{k}) = (|u_{1\mathbf{k}}\rangle, \dots, |u_{N\mathbf{k}}\rangle)$ , the non-Abelian QGT is  $\mathfrak{G}_{ij} = \partial_i u^\dagger (1 - uu^\dagger) \partial_j u$  and  $\mathcal{B}_{ij} = \text{Tr}[\mathfrak{G}_{ij}]$ . Due to its positive definiteness,  $\mathfrak{G}_{ij}$  satisfies  $\sum_{ij} c_i^\dagger \mathfrak{G}_{ij} c_j \geq 0$  for any vector  $c_i \in \mathbb{C}^2$ .

weight is then computed using linear response theory by taking the interacting Hamiltonian  $\hat{H} = \hat{H}_0 + \hat{H}_{\text{int}}$  as the unperturbed one and  $\hat{H}_1$  as the perturbing term. It can be expressed as [25]

$$D_{s,jl} = - \lim_{\mathbf{q}_\perp \rightarrow 0} \chi_{jl}(q_\parallel = 0, \mathbf{q}_\perp, \omega = 0), \quad (14)$$

where  $\chi_{jl}(\mathbf{q}, \omega)$  is a response function, that of the current induced in the system to linear order in the vector potential. In the above equation, the wavevector  $\mathbf{q} = q_\parallel \hat{l} + \mathbf{q}_\perp$  is decomposed into the collinear ( $q_\parallel$ ) and perpendicular ( $\mathbf{q}_\perp$ ) components with respect to the  $l = x, y, z$  axis.

To evaluate Eq. (14) it is necessary to resort to approximations. The typical BCS approximation is to replace the Hubbard interaction term by [5, 6]

$$\hat{H}_{\text{int}} \approx \sum_{\mathbf{i}\alpha} \left( \Delta_\alpha \hat{c}_{\mathbf{i}\alpha\uparrow}^\dagger \hat{c}_{\mathbf{i}\alpha\downarrow}^\dagger + \text{H.c.} \right). \quad (15)$$

The pairing field  $\Delta_\alpha$  is independent of the unit cell index  $\mathbf{i}$  since translational symmetry is assumed, and is calculated self-consistently as  $\Delta_\alpha = -U \langle \hat{c}_{\mathbf{i}\alpha\downarrow} \hat{c}_{\mathbf{i}\alpha\uparrow} \rangle$ , where the expectation value is taken on the ground state of the mean-field Hamiltonian

$$\hat{H}_{\text{m.f.}} = \sum_{\mathbf{k}, \alpha, \beta} \left( \hat{d}_{\mathbf{k}\alpha\uparrow}^\dagger \hat{d}_{-\mathbf{k}\alpha\downarrow} \right) H_{\alpha, \beta}(\mathbf{k}) \begin{pmatrix} \hat{d}_{\mathbf{k}\beta\uparrow} \\ \hat{d}_{-\mathbf{k}\beta\downarrow}^\dagger \end{pmatrix}, \quad (16)$$

$$H(\mathbf{k}) = \begin{pmatrix} \tilde{K}^\dagger(\mathbf{k}) - \mu & \text{diag}(\Delta_\alpha) \\ \text{diag}(\Delta_\alpha^*) & -(\tilde{K}^\downarrow(\mathbf{k}) - \mu)^* \end{pmatrix}. \quad (17)$$

Here  $\hat{d}_{\mathbf{k}\alpha\sigma} = \sum_{\mathbf{i}} e^{-i\mathbf{k} \cdot \mathbf{r}_{\mathbf{i}\alpha}} \hat{c}_{\mathbf{i}\alpha\sigma} / \sqrt{N_c}$  are field operators in momentum space with  $\mathbf{r}_{\mathbf{i}\alpha}$  the position vector of the lattice site labeled by  $\mathbf{i}\alpha$ ,  $\tilde{K}_{\alpha, \beta}^\sigma(\mathbf{k}) = \sum_{\mathbf{i}-\mathbf{j}} K_{\mathbf{i}\alpha, \mathbf{j}\beta}^\sigma e^{-i\mathbf{k} \cdot (\mathbf{r}_{\mathbf{i}\alpha} - \mathbf{r}_{\mathbf{j}\beta})}$  is the Fourier transform of the hopping matrix and  $\mu$  the chemical potential. The mean-field Hamiltonian has the block structure shown in Eq. (17) only in the case of spin rotation symmetry around a given quantization axis, which is assumed here.

For illustration purposes we consider the case in which time-reversal symmetry is present and the pairing field is real and orbital-independent  $\Delta_\alpha = \Delta$  (see Ref. 30 for a justification). Under these assumptions the superfluid weight can be written as the sum of two terms  $D_s = D_{\text{conv}} + D_{\text{geom}}$  [6, 8]. The first term reads

$$D_{\text{conv},jl} = \frac{e^2}{\hbar^2} \int \frac{d^d \mathbf{k}}{(2\pi)^d} \sum_n \left[ - \frac{\beta}{2 \cosh^2(\beta E_{n\mathbf{k}}/2)} + \frac{\tanh(\beta E_{n\mathbf{k}}/2)}{E_{n\mathbf{k}}} \right] \frac{\Delta^2}{E_{n\mathbf{k}}^2} \partial_j \varepsilon_{n\mathbf{k}} \partial_l \varepsilon_{n\mathbf{k}}, \quad (18)$$

and is called the conventional contribution to the superfluid weight since it is the sum over all bands of the result for the superfluid weight of a single-band model, Eq. (9) (now at finite temperature). In Eq. (18),  $E_{n\mathbf{k}} = \sqrt{(\varepsilon_{n\mathbf{k}} - \mu)^2 + \Delta^2}$  are the quasiparticle excitation energies (eigenvalues of  $H(\mathbf{k})$  (17)) while  $\varepsilon_{n\mathbf{k}}$  is the single-particle dispersion for the  $n$ -th band obtained from the

eigenvalue equation  $\tilde{K}^\dagger(\mathbf{k}) |u_{n\mathbf{k}}\rangle = \varepsilon_{n\mathbf{k}} |u_{n\mathbf{k}}\rangle$ . Here we use the abbreviations  $\varepsilon_{n\mathbf{k}} = \varepsilon_{n\mathbf{k}\uparrow} = \varepsilon_{n\mathbf{k}\downarrow}$  and  $|u_{n\mathbf{k}}\rangle = |u_{n\mathbf{k}\uparrow}\rangle$  because of time-reversal symmetry.

The second term is called the geometric contribution to the superfluid weight:

$$D_{\text{geom},jl} = \frac{e^2 \Delta^2}{\hbar^2} \int \frac{d^d \mathbf{k}}{(2\pi)^d} \sum_{n \neq m} \left[ \frac{\tanh(\beta E_{n\mathbf{k}}/2)}{E_{n\mathbf{k}}} - \frac{\tanh(\beta E_{m\mathbf{k}}/2)}{E_{m\mathbf{k}}} \right] \frac{(\varepsilon_{n\mathbf{k}} - \varepsilon_{m\mathbf{k}})^2}{E_{m\mathbf{k}}^2 - E_{n\mathbf{k}}^2} \times (\langle \partial_j u_{n\mathbf{k}} | u_{m\mathbf{k}} \rangle \langle u_{m\mathbf{k}} | \partial_l u_{n\mathbf{k}} \rangle + (j \leftrightarrow l)). \quad (19)$$

This contribution is a qualitatively new feature of multi-band/multiorbital lattice models and is associated to off-diagonal matrix elements of the current operator. Indeed, the current operator is represented in momentum space as  $\hat{\mathbf{J}}(\mathbf{q} = \mathbf{0}) = \frac{e}{V\hbar} \sum_{\mathbf{k}, \alpha, \beta, \sigma} \hat{d}_{\mathbf{k}\alpha\sigma}^\dagger \nabla_{\mathbf{k}} \tilde{K}_{\alpha, \beta}^\sigma(\mathbf{k}) \hat{d}_{\mathbf{k}\beta\sigma}$  and the matrix elements of  $\nabla_{\mathbf{k}} \tilde{K}^\dagger(\mathbf{k})$  have the form

$$\langle u_{m\mathbf{k}} | \nabla_{\mathbf{k}} \tilde{K}^\dagger(\mathbf{k}) | u_{n\mathbf{k}} \rangle = \nabla_{\mathbf{k}} \varepsilon_{n\mathbf{k}} \delta_{n,m} + (\varepsilon_{n\mathbf{k}} - \varepsilon_{m\mathbf{k}}) \langle u_{m\mathbf{k}} | \nabla_{\mathbf{k}} u_{n\mathbf{k}} \rangle. \quad (20)$$

This last result is used to obtain Eqs. (18)-(19). The diagonal term  $\propto \nabla_{\mathbf{k}} \varepsilon_{n\mathbf{k}}$  leads to the conventional contribution Eq. (18) and the off-diagonal term  $\propto \langle u_{m\mathbf{k}} | \nabla_{\mathbf{k}} u_{n\mathbf{k}} \rangle$  to the geometric one Eq. (19). Further details on the calculations can be found from [6, 8] and the review Ref. [31].

It is instructive to investigate the two contributions Eqs. (18)-(19) in the isolated band limit, when the chemical potential is such that a single band, denoted by  $\bar{n}$ , is partially filled and other bands are separated from it by a large band gap  $E_{\text{gap}}$ :

$$|\varepsilon_{m\mathbf{k}} - \varepsilon_{\bar{n}\mathbf{k}}| \gtrsim E_{\text{gap}} \gg U \quad \text{for } m \neq \bar{n}. \quad (21)$$

The conventional contribution in this case is just Eq. (9) with  $\varepsilon(\mathbf{k})$  replaced by  $\varepsilon_{\bar{n}\mathbf{k}}$ . On the other hand, care is required for the computation of the geometric contribution. One might expect that the geometric contribution should be vanishing in this limit since the terms of the response function that are off-diagonal in band space are suppressed by the factor  $E_{m\mathbf{k}} - E_{\bar{n}\mathbf{k}} \gtrsim E_{\text{gap}}$ , with  $m \neq \bar{n}$ , at the denominator. This would be incorrect because the off-diagonal terms of the current operator are proportional to the band gap, as seen from Eqs. (20)-(21). A careful analysis [8] shows that the geometric contribution is nonzero even in the isolated band limit and, somewhat counter-intuitively, can be expressed purely in terms of quantities relative to the partially filled band, in particular its quantum metric. This is most clearly illustrated in the case of an isolated flat band, where one obtains ( $\nu$  is the band filling) [6]

$$D_{s,jl} = D_{\text{geom},jl} = \frac{4e^2 U \nu (1 - \nu)}{N_{\text{orb}} \hbar^2} \int \frac{d^d \mathbf{k}}{(2\pi)^d} g_{jl}(\mathbf{k}), \quad (22)$$

which relates the superfluid weight to the quantum metric  $g_{jl}(\mathbf{k})$  integrated over the Brillouin zone (see Box 1).

It is clear by comparing Eq. (22) with Eq. (11) that, with some minor approximations, the nonzero superfluid weight in the flat band limit can be entirely explained in terms of the two-body bound state effective mass, Section IIB [9, 32]. The geometric contribution scales with the superconducting energy gap  $\Delta \propto U$ , while the conventional one scales roughly with the Fermi energy  $E_F$ , which is of the order of the bandwidth of the partially filled band. In usual, non-flat band, superconductors the gap  $\Delta$  is generally a much smaller energy scale than the Fermi energy and the geometric contribution is rather small.

Only very recently physical systems in which the electronic bandwidth is comparable to the superconducting gap have been realized in the laboratory, in particular magic-angle TBG (MATBG). The essential role of the off-diagonal matrix elements of the current operator was pointed out for the first time in Ref. 33 in the case of the exciton superfluid phase occurring in quantum Hall bilayers, which can be considered the first example of a flat band superfluid observed experimentally. Moreover, Kopnin showed theoretically that the superfluid weight is nonzero in the case of the flat band of surface states present in rhombohedral graphene [34]. However, these have apparently been regarded as system-specific findings until general results connecting superfluidity with quantum geometry, such as Eqs. (19) and (22), were obtained [6, 8].

#### D. Flat band superconductivity and Wannier function overlap

A natural question raised by Eq. (22) is what property of the flat band wave-functions is captured by the quantum metric and why it affects transport and superfluidity. The physical interpretation of the quantum metric can be most easily provided by Wannier functions, that is, Fourier transforms of the Bloch states

$$w_n(\mathbf{i}, \alpha) = \frac{\Omega_c}{(2\pi)^2} \int d^d \mathbf{k} e^{i\mathbf{k} \cdot \mathbf{r}_{i\alpha}} u_{n\mathbf{k}}(\alpha). \quad (23)$$

A common prescription to choose a gauge for the Wannier functions is the one based on the Marzari-Vanderbilt localization functional whose minimization leads to the maximally localized Wannier functions [35]. The gauge-invariant part of the localization functional is the trace of the quantum metric integrated over the BZ, which sets a lower bound on how much the Wannier functions can be localized. It was shown in Ref. 30 that a flat band superconductor can be described by an effective spin Hamiltonian whose exchange couplings are controlled by the overlap of the Wannier functions, which in turn is related to the Marzari-Vanderbilt functional and thus to the quantum metric. This provides a solid basis for the interpretation of the quantum metric as an invariant measure of the overlap/spread of the flat band wave functions.

Topological invariants that describe the electronic band structure provide an obstruction to the full localization of Wannier functions. An important topological invariant is the Chern number  $\mathcal{C}$  [36], see Box 1. From the positive semi-definiteness of the quantum geometric tensor one obtains the inequality

$$\det \mathcal{M}^R \geq \mathcal{C}^2, \text{ with } \mathcal{M}_{ij}^R = \frac{1}{2\pi} \int d^2 \mathbf{k} g_{ij}(\mathbf{k}). \quad (24)$$

A nonzero Chern number hence also bounds the superfluid weight, since the matrix  $\mathcal{M}^R$  is precisely the integrated quantum metric that enters in Eq. (22). This is explained by the fact that if the Chern number is nonzero one cannot find exponentially localized Wannier functions [37, 38]; at best the Wannier states are algebraically decaying with a known exponent  $1/r^2$  [39]. Such wave functions are necessarily overlapping and thus are expected to support a robust superfluid state in the isolated flat band limit.

Inequalities similar to Eq. (24) have been discovered in the case of two more topological invariants: the winding number in  $d = 1$  [30], and the Euler class in  $d = 2$  [40] which is relevant for MATBG and will be discussed in detail in the following. One expects such bound identities to exist for every topologically nontrivial band. Topology is a sufficient but not necessary condition for non-zero superfluid weight [7], because the quantum metric can be non-zero for zero Chern number, even zero Berry curvature bands – a bound that describes also such bands was recently defined using obstructed Wannier centers [41].

#### E. Berezinskii-Kosterlitz-Thouless (BKT) temperature of superconductivity in a flat band

The superfluid weight controls the susceptibility of the order parameter phase to thermal fluctuations, as seen from Eq. (8), and thus it is expected to affect the critical temperature of superconductivity. However, this effect is not captured by BCS theory in its simplest form since the order parameter  $\Delta(\mathbf{r})$  is a non-fluctuating quantity at the mean-field level. In  $d = 2$  the relation between critical temperature and superfluid weight can be made precise thanks to the universal relation  $T_{\text{BKT}} = \frac{\pi \hbar^2}{8e^2} D_s(T_{\text{BKT}})$  [42], where  $T_{\text{BKT}}$  is the Berezinskii-Kosterlitz-Thouless (BKT) temperature, that is the critical temperature of a two-dimensional superfluid, and  $D_s(T_{\text{BKT}})$  is the superfluid weight slightly below the same temperature. For an isolated flat band one obtains that  $T_{\text{BKT}} \sim U$  [6, 8], that is, the same linear dependence on  $U$  as for the BCS critical temperature in a flat band. The BKT temperature saturates for an interaction strength of the order of the band gap  $U \sim E_{\text{gap}}$  and then decreases as  $U^{-1}$  in the strong-coupling limit. This behavior can be understood with a strong-coupling expansion in which the Cooper pairs are tightly bound and move in the lattice with an effective hopping  $J \sim t^2/U$ , with  $t$  the scale of the single particle hopping [8]. The linear dependence of the critical temperature and of the superfluid weight with

the interaction strength for  $U \lesssim E_{\text{gap}}$  is a robust result that has been verified using advanced many-body methods such as dynamical mean-field theory [7, 8], quantum Monte Carlo [43, 44], and density matrix renormalization group [45–47].

### III. SUPERFLUIDITY AND TOPOLOGY IN TWISTED BILAYER GRAPHENE (TBG)

Remarkable interacting phases have been observed in TBG when the two layers are twisted with respect to each other by a "magic" angle  $\theta \approx 1.1^\circ$ , see Fig. 2a. These phases include correlated (sometimes Chern) insulators at integer filling  $\nu$  of a set of 8 (2 per valley per spin quantum numbers) flat bands around charge neutrality, with superconductors for fillings in between [40, 48–94], see Fig. 2b. Scanning tunneling microscopy (STM) experiments reveal a Coulomb repulsion strength ( $\sim 25\text{meV}$ ) [57] larger than the electron bandwidths. The strongly correlated insulators [57] at integer filling  $\nu \in [-4, 4]$  measured from charge neutrality acquire Chern numbers  $\pm(4-|\nu|)$  [56, 59–62]. Theoretically, the interacting TBG [40, 75–90], is governed by [75] an approximate  $U(4)$  symmetry (later extended to  $U(4) \times U(4)$  [68, 89]). The correlated insulator phases can be understood as ferromagnets of this large symmetry group [75, 76, 89, 95].

#### A. TBG superconductivity

Tantalizingly, moiré materials host superconductivity [50, 52, 54, 96, 97] even at the – by far – lowest densities ever:  $10^{10} - 10^{12}\text{cm}^{-2}$  [96, 97], which for the sample sizes used means 1000-10000 electrons. What causes  $\approx 1 - 5\text{K}$  superconductivity in this most dilute of all known systems? Clear evidence links superconductivity in TBG to the presence of flat bands at the magic angle. Away from these angles, superconductivity disappears. Regardless of the mechanism of TBG superconductivity, since the TBG flat bands exhibit zero total Chern number, is there a bound on their superfluid weight? What influence could the quantum geometry of the TBG bands have on the superfluid weight of TBG?

The moiré unit cell contains tens of thousands of atomic sites for small angles; such a large number of bands is unpractical to handle in most calculations. Fortunately, many approximate approaches exist. At low energies, the single particle TBG flat bands are well described by the Bistritzer-MacDonald (BM) model [48]. This model describes the coupling of the band structures of the top and bottom layers, which are rotated with respect to each other by  $\pm\theta/2$  around the  $z$ -axis. Each band structure separately consists of two Dirac points at the time-reversal ( $T$ ) partner momenta  $K$  and  $K'$  of the single layer graphene BZ (for illustrations of the BZs see Fig. 2c). When  $\theta$  is small such that the interlayer coupling is smooth in real space (with a length scale

of variation much larger than the atom distances), the graphene valley ( $K$  and  $K'$ ) is a good quantum number of low energy states of TBG [48] and due to its conservation the Dirac states around  $K$  ( $K'$ ) in the top layer only couple to the states around  $K$  ( $K'$ ) in the bottom layer. The Dirac Hamiltonian around  $K$  in the top layer is  $-iv_F\partial_x(\cos\frac{\theta}{2}\sigma_x - \sin\frac{\theta}{2}\sigma_y) - iv_F\partial_y(\cos\frac{\theta}{2}\sigma_y + \sin\frac{\theta}{2}\sigma_x) \approx -iv_F\partial_{\mathbf{r}} \cdot \boldsymbol{\sigma} + i\frac{\theta}{2}v_F\partial_{\mathbf{r}} \times \boldsymbol{\sigma}$ , where  $v_F$  is the Fermi-velocity of single-layer graphene and  $\boldsymbol{\sigma} = (\sigma_x, \sigma_y)$  are Pauli matrices representing the A/B sublattices of graphene. For the bottom layer we replace  $\theta \rightarrow -\theta$ . The interlayer coupling is encoded in a position-dependent matrix  $T(\mathbf{r})$ , such that the Hamiltonian of TBG, at valley  $K$ , can be written as

$$H(\mathbf{r}) = -iv_F\tau_0\partial_{\mathbf{r}} \cdot \boldsymbol{\sigma} - \frac{\theta}{2}\tau_z\partial_{\mathbf{r}} \times \boldsymbol{\sigma} + \begin{pmatrix} 0 & T(\mathbf{r}) \\ T^\dagger(\mathbf{r}) & 0 \end{pmatrix}. \quad (25)$$

Here  $\tau_0$  and  $\tau_z$  are the identity and the third Pauli matrix for the layer degree of freedom, respectively. Ref. [48] derived  $T(\mathbf{r})$  for small  $\theta \sim 1^\circ$ :

$$T(\mathbf{r}) = \sum_{i=1}^3 e^{-i\mathbf{q}_i \cdot \mathbf{r}} T_i, \quad (26)$$

where  $\mathbf{q}_i$ 's are  $\mathbf{q}_1 = k_D(0, -1)$ ,  $\mathbf{q}_2 = k_D(\frac{\sqrt{3}}{2}, \frac{1}{2})$ ,  $\mathbf{q}_3 = k_D(-\frac{\sqrt{3}}{2}, \frac{1}{2})$ , with  $k_D = 2|K|\sin\frac{\theta}{2}$  being the distance between  $K$  momenta in the two layers, and  $v_F = 5.944\text{eV} \cdot \text{\AA}$ ,  $|K| = 1.703\text{\AA}^{-1}$ . The  $T_i$ 's are

$$T_i = w_0\sigma_0 + w_1 \left[ \sigma_x \cos \frac{2\pi(i-1)}{3} + \sigma_y \sin \frac{2\pi(i-1)}{3} \right], \quad (27)$$

where the AA and AB hopping are  $w_1 = 110\text{meV}$ ,  $w_0 = 0.7w_1$ , respectively. The translation symmetry of the moiré potential Eq. (26) under the moiré unit cell translations  $\mathbf{a}_{M1} = \frac{2\pi}{k_D}(\frac{1}{\sqrt{3}}, \frac{1}{3})$ ,  $\mathbf{a}_{M2} = \frac{2\pi}{k_D}(-\frac{1}{\sqrt{3}}, \frac{1}{3})$  is manifest in real space, see Fig. 2c. At  $\theta \approx 1.1^\circ$ , two very flat bands can be seen in Fig. 2d (marked with blue); these are conventionally referred to as the "active bands" of TBG.

#### B. The BKT temperature and geometric contribution in TBG

Being near the BKT transition is manifested in electron transport as  $V \propto I^3$  dependence between the longitudinal voltage  $V$  and the current  $I$ . Using this,  $T_{\text{BKT}}$  was estimated in Ref. [50] to be about 1 K, however, the fit to  $I^3$  was partial. In a more recent work on magic-angle twisted *trilayer* graphene, a clear  $I^3$  behaviour was observed, giving  $T_{\text{BKT}} \simeq 2.1\text{K}$  [98].

Theoretically, the BKT temperature of TBG superconductors was estimated for the first time in Refs. [40, 78, 79]; for a brief introduction see [99]. Ref. [79] utilized the low-energy BM model described above and considered local  $s$ -wave pairing leading to a local mean-field order



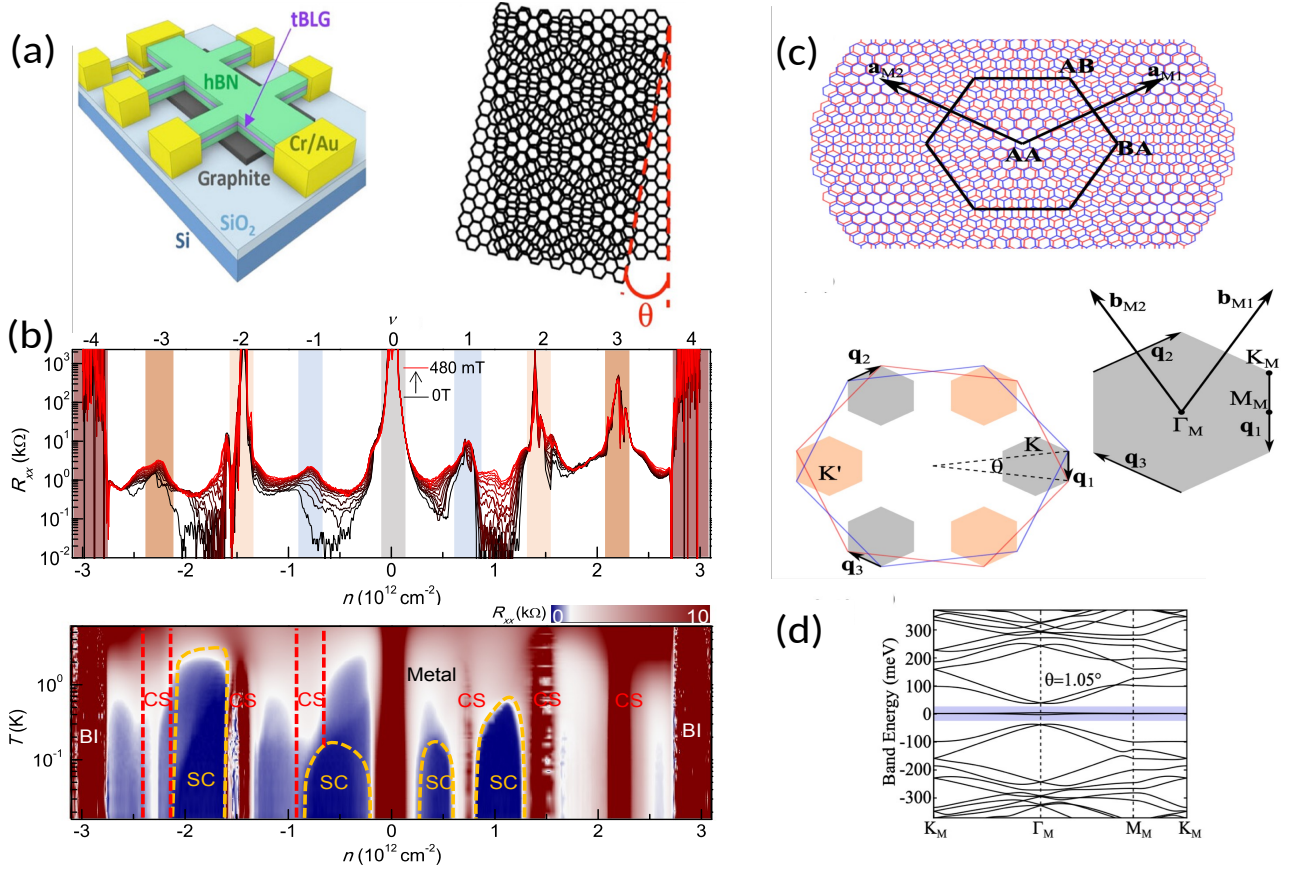


**Figure 2. TBG lattice, experimental phase diagram, and band structures.** (a) Sample for encapsulated moiré TBG (tBLG in the picture) lattice for a rotation angle  $\theta$ . (b) Experimental observation of correlated insulators (correlated states, CS) – the red regions of the plots where the resistance ( $R_{xx}$ ) peaks – at integer fillings  $\nu$  of the two flat bands shaded in (d), and superconducting (SC) phases (low resistance regions in blue) in between the insulating phases, and band insulators (BI). Here  $T$  is the temperature and  $n$  is the density. Obtained with permission from [51]. (c) Top: The moiré unit cell, where the blue sheet and the red sheet represent the top and bottom layers, respectively. In the AA, AB, BA regions, the A sublattice of the top layer are located above the A sublattice, the B sublattice, and the hexagon center of the bottom layer, respectively. Bottom: the moiré BZ. Left: The grey and yellow hexagons represent the moiré BZ for the graphene valleys  $K$  and  $K'$ , respectively. Right: The reciprocal lattices and the high symmetry momenta of the moiré BZ in graphene valley  $K$ . (d) The band structure of the magic-angle  $\theta = 1.05^\circ$  TBG with its two flat bands (for one valley) using the BM model.

parameter  $\Delta$ . Ref. [78] presents a more microscopic approach where the full tight-binding TBG Hamiltonian is reduced to a model that is manageable but still has a large unit cell of a few hundreds of atoms, by using the so-called renormalization moiré (RM) method [100, 101]. A low-energy continuum calculation was presented as a comparison to the RM calculations. Both local  $s$ -wave and nearest-neighbour resonance valence bond (RVB) pairing were considered, in the latter the order parameter  $\Delta$  corresponds to pairing of electrons in neighbouring sites. Both works [79] and [78] found that  $T_{\text{BKT}}$  at the magic angle is significantly influenced by the geometric contribution of superconductivity Eq. (19). In Ref. [79] it was shown that the geometric contribution to the superfluid weight is about twice as large than the conventional one at the magic angle, while slightly away from it the conventional one starts to dominate, see Fig. 3(a-b). As the pairing mechanism and the interaction strength in TBG

are not precisely known at the moment, no accurate predictions of  $T_{\text{BKT}}$  could be made in Refs. [40, 78, 79], however, the estimates gave temperatures in the few Kelvin range, consistent with the experiments. Assuming  $\Delta(T) \approx 2k_B T_c^* (1 - T/T_c^*)^{1/2}$  [23], the ratio between the Cooper pair formation (BCS) critical temperature  $T_c^*$  and  $T_{\text{BKT}}$  was found for the filling ratio  $\nu = 1/4$  (2 electrons per moiré unit cell) to be  $T_{\text{BKT}}/T_c^* = 0.35$ . For the geometric contribution of the TBG superfluid weight  $D_s$  at zero temperature, using the experimental  $T_{\text{BKT}} = 1.5$  K [50] and an order parameter  $\Delta = 2k_B T_c^* \approx 0.74$  meV, the value  $[D_s]_{\text{geom}} \approx \frac{4e^2 \Delta}{\pi \hbar^2} \sqrt{\nu(1-\nu)} \approx 1.5 \times 10^8 \text{ H}^{-1}$  was obtained [40, 78, 79]. This is *one* order of magnitude smaller than the superfluid weight in BSCCO and MoGe, but for a TBG density *two* orders of magnitude smaller ( $n \approx 10^{12} \text{ cm}^{-2}$ ).

TBG superconductivity is often described by models fea-

turing only the four nearly flat bands, as it is assumed that the low-energy physics dominates. Importantly, however, the work [78] suggests that neglecting higher bands may not be adequate when calculating the BKT temperature; the underlying reason is that the geometric contribution of the superfluid weight is due to interband processes which do *not* scale as one over the band gap as one might naively expect for processes involving higher bands (see Eqs. (19), (20), and Ref. [8]). Fig. 3(c-d) shows how the TBG superfluid weight divides into the conventional and geometric contributions, the latter becoming dominant when interactions exceed the bandwidth, that is, the flat band regime is approached. Fig. 3(c-d) makes clear that considerably more than four bands need to be included to get quantitatively or even qualitatively correct results. One more finding in [78] was that, in case of the RVB pairing, the superfluid is nematic and the corresponding superfluid weight anisotropic – thus measurements of the superfluid weight could distinguish between local or non-local pairing mechanism through (an)isotropy.

The linear dependence of the BKT temperature on interaction in case of TBG was confirmed by Monte Carlo calculations [44]. The same was found to hold for the temperatures where the single-particle density of states and the spin susceptibility reach their maxima. These temperatures were higher than the BKT temperature, indicating singlet and gap formation already above the temperature for superconductivity. Such pseudogap formation was also studied in Ref. [102] for a flat band model different from TBG. It was pointed out that the ratio between the pseudogap temperature and  $T_{\text{BKT}}$  can tell about the geometric contribution of the preformed pair effective mass.

Besides moiré materials, the geometric contribution to the superfluid weight has been found to be important in another 2D superconductor, monolayer FeSe grown on a SrTiO<sub>3</sub> (STO) substrate [103], which has a critical temperature of 65K. FeSe on STO has a large ratio  $T_c/T_F \sim 0.1$  between critical temperature and Fermi temperature, even larger than that of TBG [50] (a property shared with its parent compound: bulk FeSe [104]). These findings validate the general picture that the effect of quantum geometry on superfluidity is crucial in materials close to the flat band limit.

### C. Symmetries of TBG, Fragile and stable topology

The TBG eigenstates exhibit subtle topology of either a "fragile" or stable type depending on the symmetries kept in the model. The single-graphene-valley Hamiltonian Eq. (25) has the symmetries of the magnetic space group  $P6'2'2$  [69] (#177.151 in the BNS setting [105]): (i)  $C_{2z}T = \sigma_x K$ , where  $K$  is the complex conjugation, (ii)  $C_{3z} = e^{i\frac{2\pi}{3}\sigma_z}$ , (iii)  $C_{2x} = \tau_x \sigma_x$ .  $C_{2z}$  rotation and the time-reversal  $T$  separately are not symmetries of Eq. (25) since they map the graphene valley  $K$  into  $K'$ . A non-crystalline important symmetry for a small twist angle is

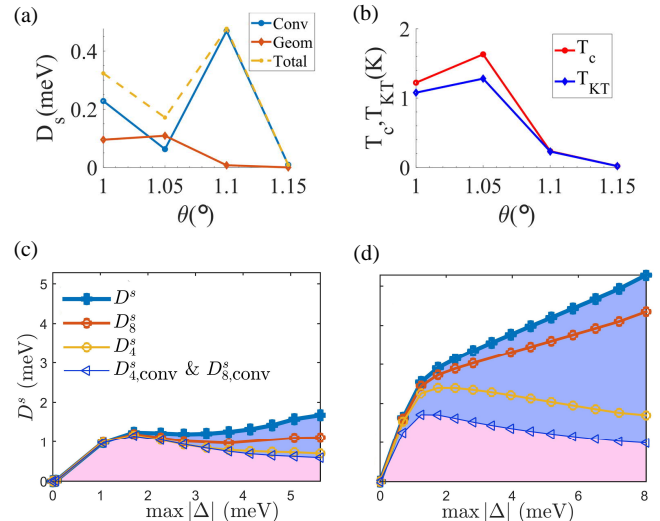


**Figure 3. Geometric contribution in TBG superfluid weight.** Superfluid weight  $D_s$  (a) and the critical temperature (b) calculated in [79], as function of the twist angle  $\theta$ . The geometric contribution of  $D_s$  is larger than the conventional one at the magic angle  $1.05^\circ$  while away from it the conventional one dominates; the critical temperature changes from BKT type ( $T_{KT}$ ) to the conventional BCS one ( $T_c$ ) when moving away from the magic angle. (c-d) Superfluid weight as a function of the order parameter (as it is spatially varying, maximum  $\Delta$  is used), from [78]. (c) is for the nearest neighbor (RVB) interaction and (d) for local. For interactions large compared to the bandwidth, the flat band limit is reached and the geometric contribution (blue area) becomes larger than the conventional one (pink). The lines marked with different symbols show that the conventional contribution is well captured by including only the four lowest bands in the calculation, while more than eight are needed to the correct result in the case of the geometric contribution which arises from interband processes. Figures obtained from [79] and [78] with permission.

a unitary particle-hole inversion operation  $P = i\tau_y$ , for which  $PH(\mathbf{r})P^\dagger = -H(-\mathbf{r})$ . Crucially, Ref. [69] proved that these symmetries force the single-valley TBG model to be topological at any *small* twist angle and that the active bands of TBG *cannot* be described by localized symmetric Wannier states. To explain that, remind that the Wannier functions  $w_n(\mathbf{i}, \alpha)$ , Eq. (23), are spread in space ( $\mathbf{i}, \alpha$  are the unit cell and orbital indices). One can define the “center” of the Wannier function as the average location, measured from the origin; scaled by the unit length, this corresponds to the Berry phase [11, 106]. If one Fourier transforms (Eq. (23)) with  $k_y$  only, the Wannier center in the  $y$  direction will depend on  $k_x$ . This motion of the Wannier center as a function of the BZ momentum  $k_x \in [0, 2\pi)$  is called the Wilson loop [11, 106] and is shown for TBG in Fig. 4a. Importantly, it winds between  $\pi$  and  $-\pi$ . This means that the Wannier functions cannot be simultaneously localized in  $x$  and  $y$ : such localization would imply the  $y$  Wannier center cannot move across the entire  $y$ -unit cell as  $k_x$  is varied across

the BZ.

The type of topology that the valley-filtered bands respect has been subject to revision. In the initial papers [65, 68–70, 107, 108] the topology was thought to be of a new, "fragile" type [72, 109, 110] protected by  $C_{2z}T$  (this type of topology does not require any of the other symmetries of TBG). Fragile topology is an obstruction to constructing symmetric Wannier functions for a given set of bands which can be *removed* by adding other topologically *trivial* bands to the Hilbert space [109, 110]. Computing the Wilson loop of more than the two bands around charge neutrality, Fig. 4a, causes crossings at different Wilson eigenvalues (schematically shown in Fig. 4b) at any small coupling. Consequently, the Wannier center winding disappears, the band topology is trivialized, and one can construct localized Wannier functions. Very recently it was realized [93] that if one further imposes the particle-hole symmetry  $P$  on TBG, the topology becomes stable and not fragile. The combined antiunitary operator  $(PC_{2z}T)^2 = -1$  mimics the case of spinful time-reversal symmetry and protects Kramers doublets in the Wilson spectrum at  $k_1 = 0$  and  $k_1 = \pi$  [106, 111] (see Fig. 4c). The flow of the Wannier centers in TBG thus shows winding, Figs. 4c,d, and the valley- $K$  model Eq. (25) is *always* strongly topological no matter how many bands are included. Mixing the other valley renders the topology trivial; at small angles, however, the two valleys do not mix [48].

#### D. Lower bound of superconductivity in TBG from topology

The winding of the Wilson loop reflecting the topology of the active bands in TBG [69] can also be characterized by an integer-valued invariant, Euler or Stiefel–Whitney class  $e_2 = 1$  [71]. Refs. [69, 71, 93] showed this implies the existence of  $4l + 2e_2$  ( $l$  integer) Dirac nodes at zero energy between the two active bands which cannot be energetically separated. Based on Sec. IID, the superfluid weight of topological bands should be nonzero; however, the inequality bound Eq. (24) cannot be used, as the Chern number is zero due to the  $C_{2z}T$  symmetry. Instead, the symmetry class of  $(C_{2z}T)^2 = 1$  provides a new lower bound for the superfluid weight in TBG [40], using the universally true Eq. (22). The non-Abelian Berry connection and curvature of the two TBG flat bands can be written as in Box 1, under a proper *local* gauge choice on a patch in the BZ [65, 69, 70, 107]. In [40] it was proved that the Wilson loop winding number [69] is equivalent to the Euler class  $e_2$  in Ref. [107] whose expression is given in Box 1.

Using the positive definiteness of the non-Abelian QGT  $\mathfrak{G}_{ij}$  (choosing the vectors  $c_x$  and  $c_y$  in Box 1 properly), it was shown [40] that the quantum metric is bounded by the off-diagonal part  $f_{xy}$  of the non-Abelian Berry curvature  $\mathcal{F}_{xy}$ :  $\text{tr } g \geq 2|f_{xy}|$ , which in turn means that the

superfluid weight is bounded by the Euler characteristic:

$$\begin{aligned} \frac{1}{4\pi} \int_{\text{BZ}} d^2k \text{tr } g(\mathbf{k}) &\geq \frac{1}{2\pi} \int_{\text{BZ}'} d^2k |f_{xy}| \\ &\geq \left| \frac{1}{2\pi} \int_{\text{BZ}'} d^2k f_{xy} \right| = |e_2|. \end{aligned}$$

#### E. Quantum Geometry in the Correlated Insulator States of TBG

Remarkably, a generalization of the quantum metric also appears in the TBG correlated insulator states [94]. Being in the strong coupling limit, TBG interacting states of matter [40, 75–90] depend chiefly on the eigenstates (but not the energies) of the flat bands. The insulating states in TBG at integer filling are amongst the best studied experimentally and theoretically, and the least theoretically controversial as extensive theoretical efforts have been aimed at their explanation [75–77, 80–90].

The strong coupling TBG Coulomb Hamiltonians of Kang and Vafeek [75] and others [65, 95, 112, 113] (similarly to the negative  $U$  projected Hubbard models in the superfluid weight), allow for exact expressions of energy and eigenstate of the charge  $\pm 1$  excitation (relevant for transport gaps), of neutral excitation, and of charge  $\pm 2$  excitation (relevant for possible Cooper pair binding energy [89, 95]). Ref. [89, 95] found that the charge 1 excitation dispersion is governed by a generalized quantum geometric tensor of the projected bands, convoluted with the Coulomb interaction. Hence the quantum geometric tensor influences the charge excitation dispersion of the insulating states of TBG, similar to how it governs the Cooper pair dispersion for the attractive Hubbard model.

### IV. MULTILAYERS AND FLAT BANDS IN ULTRACOLD GASES

Atoms trapped by magnetic fields and light-induced potentials can be cooled to extremely low temperature, and by means of laser standing waves it is possible to force the atoms to move on the discrete lattice formed by the local minima of the optical potential, thereby mimicking the lattice of atomic orbitals in solids [115–118]. These so-called optical lattices are just one example of the high degree of tunability of ultracold gases, which makes them an excellent quantum simulation platform to tackle currently intractable problems in quantum many-body physics and condensed matter physics. After the realization of Bose-Einstein condensates and quantum degenerate Fermi gases, experiments with ultracold gas have become increasingly sophisticated. The rich and versatile ultracold gas experimental toolbox has allowed to realize, among other things, artificial graphene lattices [119, 120], geometries displaying flat bands like kagome [121] and Lieb [122] lattices and synthetic dimensions [123–125].



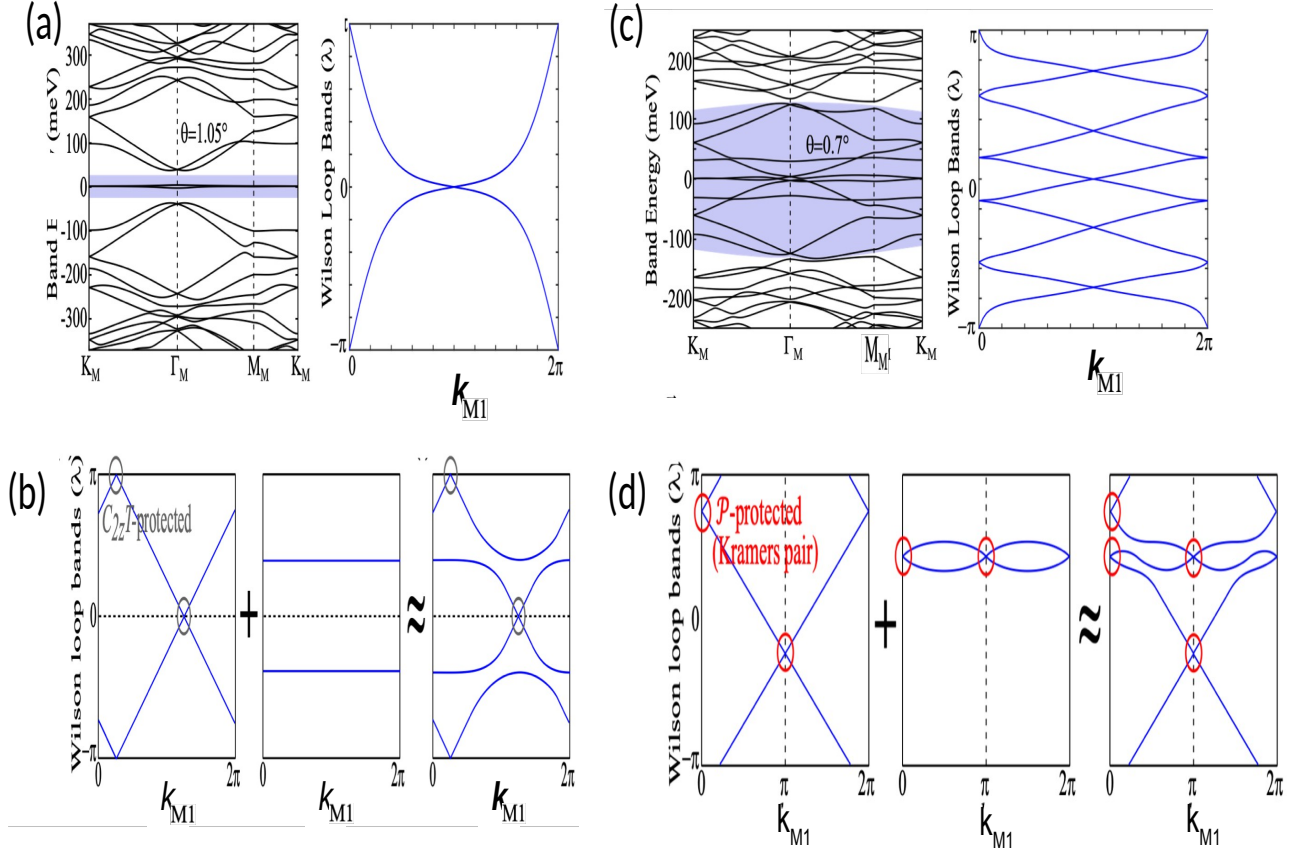


Figure 4. **Wilson loops/Wannier centers, fragile and stable topology of TBG.** (a) Left: The band structure of the magic-angle  $\theta = 1.05^\circ$  TBG with its two flat bands (using the BM model, single valley). Right: their hybrid Wannier centers – the Wilson loop bands. The crossings in the Wilson loop bands are protected by  $C_{2z}T$  and/or the approximate  $\mathcal{P}$  symmetries. Each Wilson loop operator is integrated along  $\mathbf{b}_{M2}$  (definition in Fig. 2(c)) and the spectrum is plotted along  $\mathbf{b}_{M1}$ . (b) The Wilson loop bands with  $C_{2z}T$ . The crossings at  $\lambda = 0, \pi$  are protected by  $C_{2z}T$ . For a two-band system, the topology is nontrivial if the Wilson loop bands – representing the position of the Wannier center – wind (left) across the unit cell and is trivial otherwise (middle and right). The  $C_{2z}T$ -protected topology is fragile: Coupling the nontrivial Wilson loop bands (left) to a trivial Wilson loop bands (right), as the bands do not wind over the whole BZ any more. (c) The band structure (left) and Wilson loop bands (right) of the middle ten bands of TBG (shaded) at  $\theta = 0.7^\circ$ . The crossings at  $\lambda = 0, \pi$  in the Wilson loop bands are protected by  $C_{2z}T$  and/or by particle-hole  $P$ ; the double degeneracies with  $\lambda \neq 0, \pi$  at  $k_1 = 0, \pi$  are protected by the approximate  $\mathcal{P}$  symmetry. These double-degeneracies guarantee winding of the Wilson loops across the BZ for any bands with  $4n + 2$  Dirac nodes at zero energy. The parameters of the Hamiltonian used in (a-d) are  $v_F = 5.944\text{eV} \cdot \text{\AA}$ ,  $|K| = 1.703\text{\AA}^{-1}$ ,  $w_1 = 110\text{meV}$ ,  $w_0 = 0.7w_1$ . (d) Comparison of Wilson loop windings protected by  $\mathcal{P}$  and  $C_{2z}T$ . The crossings at  $k_{M1} = 0, \pi$  are Kramers pairs protected by  $\mathcal{P}$ . The  $Z_2$  Euler invariant equals to 1 if the Wilson loop bands form a zigzag connection between  $k_{M1} = 0$  and  $k_{M1} = \pi$  and equals to 0 otherwise. The  $\mathcal{P}$ -protected topology is stable against adding trivial bands: Coupling the nontrivial Wilson loop bands (left) to trivial Wilson loop bands (middle) yields nontrivial Wilson loop bands (right).

The phase diagram of TBG depending on the twist angle and filling is currently a hotly debated subject, and proposals have been put forward recently for realizing an ultracold gas analogue of TBG [126–128] and investigating this problem in a well-controlled setting. The central idea common to all proposals is to use the internal hyperfine states of the atoms to encode the layer degree of freedom of TBG as a synthetic dimension. In practice this means that the optical potential depends on the hyperfine state. There are different methods to realize a state-dependent optical potential, but they all rely on a clever arrangement

of the laser field polarizations and the level structure of the atoms [126]. The interlayer tunneling is engineered either by coupling the two states directly with microwave radiation or by a two-photon Raman transition. The proposals differ on how the moiré pattern is realized: One can simply have the two optical lattices for the two states tilted with respect to each other [126]. Alternatively, it is possible to obtain the same result by spatially modulating the Raman field, if the interlayer tunneling is obtained with a two-photon Raman transition [127]. In the latter case the period of the moiré pattern is precisely the period



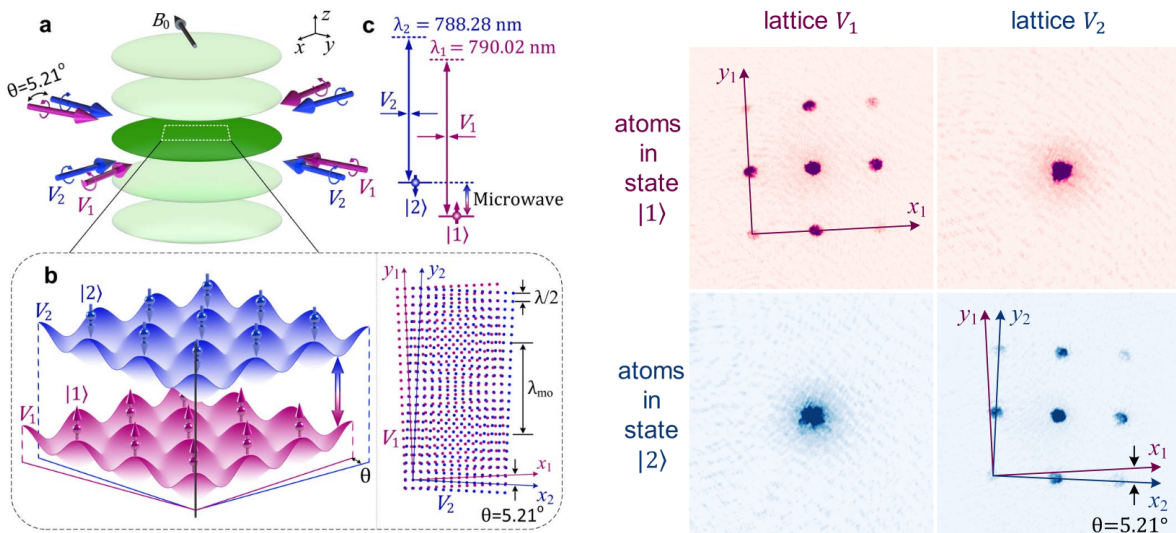


Figure 5. **Experimental realization of a twisted bilayer optical lattice.** On the left the concept of the experiment [114] is illustrated. Two hyperfine levels of  $^{87}\text{Rb}$  atoms,  $|1\rangle$  and  $|2\rangle$ , encode the “layer” degree of freedom. Since the atoms with different spin states are not spatially separated along the  $z$  axis, the layer degree of freedom is realized as a synthetic dimension. A strong confinement along the  $z$ -direction constrains the atom motion to the quasi-2D regime, and all atoms are trapped in the dark green pancake in panel a. The twisted bilayer is created by 2D square optical lattices  $V_1$  and  $V_2$ , which are rotated with respect to each other by an angle  $\theta$ , as seen in panel b. The wavelengths and the polarizations of the two lattices are fine-tuned in such a way that atoms in spin state  $|1\rangle$  ( $|2\rangle$ ) feel only the  $V_1$  ( $V_2$ ) lattice. As seen from the time-of-flight images on the right side, a matter wave of atoms in state  $|i\rangle$  is diffracted only by the  $V_i$  lattice. The coherent tunneling between the layers is realized here by the coherent coupling of the spin states with microwave radiation (panel c). Figures reproduced with permission from Ref. [114].

of the modulation of the Raman field and one can avoid to physically twist the optical lattices.

The first strategy of tilted state-dependent optical lattices has been used in a recent experimental implementation with Rubidium-87 [114], which is illustrated in Fig. 5. Whereas  $^{87}\text{Rb}$  is bosonic, a generalization of the same scheme for fermionic atoms could allow to realize a faithful model of TBG in the near future. These recent results demonstrate that twisted bilayers are feasible within the ultracold gas toolbox, however to probe the effect of quantum geometry on superfluidity it is also necessary to measure observables such as the superfluid weight, in particular its dependence on the interaction strength. A whole set of new ideas and methods are required for measuring such observables in ultracold gases [129]. A lot of work has already been done in this sense: in the case of the unitary Fermi gas the superfluid fraction has been measured by directly imaging the density variations associated to the propagation of a wave of second sound [130], a mode characterized by out of phase oscillations of the normal and superfluid components.

Some theoretical ideas for measuring the superfluid density are a direct analog of the classical experiment with helium-II by Andronikashvili: a finite angular velocity is imparted to the ultracold gas, either by rotating the optical trap or by using a light-induced vector potential, and then the moment of inertia, directly related to the superfluid fraction, is obtained from the density

redistribution [131] or spectroscopically from the hyperfine level population [132, 133]. Other approaches based on artificial gauge fields can possibly allow to measure the superfluid density at a local level and out of equilibrium [129]. The ability to bring the ultracold gas out of equilibrium by suddenly changing a control parameter (a so-called quench) can also be useful to measure the superfluid weight in lattice systems [134, 135]. Another route to probe the transport properties in a rather direct fashion is to realize atomtronic two-terminal setups [136, 137], such as the one that has allowed to observe superfluid flow in the presence of disorder [138]. In a two-terminal setup superfluid transport can be probed through the Josephson effect for instance [139].

## V. OUTLOOK

The fingerprint of quantum geometric flat band superconductivity is the linear dependence on the interaction of the following quantities: Cooper pairing temperature, the pairing gap, superfluid weight, and the BKT superfluid transition temperature. Experiments where (at least some of) these quantities are measured while varying the interaction would reveal – if approximately linear dependence is seen – the geometric contribution of superfluidity for the first time. The normal state above the critical temperature is also likely to reveal interesting preformed

pair, pseudogap or insulator behavior characteristic for a flat band [44, 45, 102, 140].

As platforms, the 2D moiré materials [18–22] and ultracold gases [115–118] are complementary. Although remarkable demonstration on tuning the electronic interactions via electric field exists in twisted graphene [98], in general the control of interaction is easier and more precise in ultracold gases. There, the Feshbach resonance technique allows realizing negative or positive interaction strengths of any magnitude, without affecting any other system parameter. The microscopic interaction is well approximated by a contact interaction, allowing to test Hubbard-type theories precisely. Another advantage of ultracold gas setups is that the ratio between inter- and intra-layer tunneling amplitudes can be adjusted more freely than in moiré materials. This opens up the possibility of observing quasi-flat bands for larger rotation angles (smaller moiré unit cells), for instance. The great advantage of the 2D materials is that the temperatures required for superconductivity can actually be reached. While continuum ultracold gases routinely show superfluidity, bringing *fermions in lattices* to the superfluid temperatures is a challenge, although advances in realizing antiferromagnetic states [141] suggest it should be reached soon. While waiting, ultracold gases suit for exploring the normal state, and bosonic superfluidity. Ultracold gases are clean systems where impurities can be added in a controllable way, so they are an excellent platform for understanding the effect of disorder. The quantum gas microscopes [117] provide direct information about the fluctuations and quantum correlations of the ground state. For TBG, revealing quantum geometry effects via noise measurements has been proposed [142]. The charge quasiparticle dispersion which is related to QGT (Section III E) can be revealed by STM. Concerning transport experiments, 2D materials are clearly the advantageous platform, although opportunities exist also in ultracold gases [137, 139].

Superconductivity in TBG is obviously only the beginning. Another promising moiré material is  $\text{WTe}_2$ , where a topological exciton insulator has been observed in single layer [143] but where metallic behavior is obtained in moiré bilayers [144]; the appearance of superconductivity at some twist angles in  $\text{WTe}_2$  would be interesting due to its topological bands. Transition to the superconducting state has been observed already in magic angle twisted trilayer graphene (MATTG) [98]. Remarkably, the transition temperature in MATTG was more than 2 K, larger than in MATBG. Would stacking more layers eventually lead to room temperature superconductivity, in the spirit of the early proposal [2]? Certainly, materials which have been thought to be non-superconducting in the past – such as untwisted graphene, become superconducting when three layers are stacked together [145]. In principle, the critical temperature seems not to have a general upper bound [146], although limits exist for specific cases [147]. Due to the fundamental lower bound of superfluidity Eqs. (22), (24), one can expect higher

critical temperatures for large quantum metric, or Chern number. However, these results assume the isolated flat band limit; the quantum metric typically diverges when bringing other bands close to the flat band. While the divergence does not show up in the superfluid weight (due to the contribution of other bands), it still leads in general to the enhancement of the latter [7]. This hints to a possible sweet spot where quantum geometry effects are maximized by bringing other bands close to the flat band, while keeping them far enough so that most of the pairing takes place in the flat band where interactions dominate.

The quantum metric is a fundamental quantity describing distances between the eigenstates of a system, and hence appears in many observables of interacting systems. For instance, light-matter interactions in TBG reflect the underlying quantum geometry as well [148, 149]. Recently, quantum geometry was predicted to stabilize Bose-Einstein condensates in flat bands [150], relevant for bosonic condensates in ultracold gas and polariton systems, or even for 2D moiré materials at the bosonic end of the BCS-BEC crossover [98].

## KEY POINTS

- Bands of (quasi)flat dispersion dramatically enhance Cooper pairing as their (nearly-)vanishing kinetic energy allows interaction effects to dominate.
- Superfluidity and stable supercurrents are possible in a flat band if the band has non-trivial quantum geometry: the related overlap of the Wannier functions facilitates movement of interacting particles even when non-interacting particles would be localized.
- Twisted bilayer graphene (TBG) exhibits nearly flat bands at its Fermi energy for small twist angles. Theory work suggests that quantum geometry is essential for the experimentally observed TBG superconductivity, and that a topological invariant called Euler class provides a lower bound for its superfluid weight.
- Ultracold gases offer another promising platform for highly controllable studies of superfluidity in moiré geometries. The first experiments are on the way.
- A flat band dispersion together with a quantum geometry that guarantees superfluidity are powerful guidelines for the search of superconductivity at elevated temperatures.

## ACKNOWLEDGMENTS

S.P. and P.T. acknowledge support by the Academy of Finland under project numbers 330384, 336369, 303351, and 327293. B.A.B. acknowledges support from the Office of Naval Research grant No. N00014-20-1-2303 and from the European Research Council (ERC) under the European Union's Horizon 2020 research and innovation programme (grant agreement n° 101020833).

## AUTHOR CONTRIBUTIONS

All authors have contributed to the writing of the manuscript.

## COMPETING INTERESTS

The authors declare no competing interests.

- 
- [1] X. Zhou, W.-S. Lee, M. Imada, N. Trivedi, P. Phillips, H.-Y. Kee, P. Törmä, and M. Eremets, High-temperature superconductivity, *Nature Reviews Physics* **3**, 462 (2021).
  - [2] N. Kopnin, T. Heikkilä, and G. Volovik, High-temperature surface superconductivity in topological flat-band systems, *Phys. Rev. B* **83**, 220503 (2011).
  - [3] T. Heikkilä, N. Kopnin, and G. Volovik, Flat bands in topological media, *Pis'ma ZhETF* **94**, 233 (2011).
  - [4] V. A. Khodel' and V. R. Shaginyan, New approach in the microscopic Fermi systems theory, *Physics Reports* **249**, 1 (1994).
  - [5] J. R. Schrieffer, *Theory of Superconductivity*, Frontiers in Physics (Benjamin, New York, 1964).
  - [6] S. Peotta and P. Törmä, Superfluidity in topologically nontrivial flat bands, *Nature Communications* **6**, 8944 (2015).
  - [7] A. Julku, S. Peotta, T. I. Vanhala, D.-H. Kim, and P. Törmä, Geometric origin of superfluidity in the Lieb lattice flat band, *Phys. Rev. Lett.* **117**, 045303 (2016).
  - [8] L. Liang, T. I. Vanhala, S. Peotta, T. Siro, A. Harju, and P. Törmä, Band geometry, Berry curvature and superfluid weight, *Phys. Rev. B* **95**, 024515 (2017).
  - [9] P. Törmä, L. Liang, and S. Peotta, Quantum metric and effective mass of a two-body bound state in a flat band, *Phys. Rev. B* **98**, 220511 (2018).
  - [10] J. P. Provost and G. Vallee, Riemannian Structure on Manifolds of Quantum States, *Commun. Math. Phys.* **76**, 289 (1980).
  - [11] R. Resta, The insulating state of matter: A geometrical theory, *Eur. Phys. J. B* **79**, 121 (2011).
  - [12] M. Z. Hasan and C. L. Kane, Colloquium: Topological insulators, *Rev. Mod. Phys.* **82**, 3045 (2010).
  - [13] B. A. Bernevig and T. L. Hughes, *Topological Insulators and Topological Superconductors* (Princeton University Press, 2013).
  - [14] A. Mielke, Ferromagnetic ground states for the Hubbard model on line graphs, *J. Phys. A: Math. and Gen.* **24**, 2 (1991).
  - [15] E. H. Lieb, Two theorems on the Hubbard model, *Phys. Rev. Lett.* **62**, 1201 (1989).
  - [16] D. Leykam, A. Andreanov, and S. Flach, Artificial flat band systems: from lattice models to experiments, *Advances in Physics: X* **3**, 1473052 (2018).
  - [17] D. Călugăru, A. Chew, L. Elcoro, N. Regnault, Z.-D. Song, and B. A. Bernevig, General construction and topological classification of all magnetic and non-magnetic flat bands, (2021), [arXiv:2106.05272](https://arxiv.org/abs/2106.05272) [cond-mat.mes-hall].
  - [18] A. H. MacDonald, Bilayer graphene's wicked, twisted road, *Physics* **10.1103/Physics.12.12** (2019).
  - [19] E. Y. Andrei and A. H. MacDonald, Graphene bilayers with a twist, *Nature Materials* **19**, 1265 (2020).
  - [20] L. Balents, C. R. Dean, D. K. Efetov, and A. F. Young, Superconductivity and strong correlations in moiré flat bands, *Nature Physics* **16**, 725 (2020).
  - [21] D. M. Kennes, M. Claassen, L. Xian, A. Georges, A. J. Millis, J. Hone, C. R. Dean, D. N. Basov, A. N. Pasupathy, and A. Rubio, Moiré heterostructures as a condensed-matter quantum simulator, *Nature Physics* **17**, 155 (2021).
  - [22] E. Y. Andrei, D. K. Efetov, P. Jarillo-Herrero, A. H. MacDonald, K. F. Mak, T. Senthil, E. Tutuc, A. Yazdani, and A. F. Young, The marvels of moiré materials, *Nature Reviews Materials* **6**, 201 (2021).
  - [23] M. Tinkham, *Introduction to Superconductivity*, 2nd ed. (Dover Publications, Mineola, N.Y., 2004).
  - [24] D. Scalapino, S. R. White, and S. C. Zhang, Superfluid density and the Drude weight of the Hubbard model, *Phys. Rev. Lett.* **68**, 2830 (1992).
  - [25] D. Scalapino, S. R. White, and S. C. Zhang, Insulator, metal, or superconductor: The criteria, *Phys. Rev. B* , 7995 (1993).
  - [26] B. S. Chandrasekhar and D. Einzel, The superconducting penetration depth from the semiclassical model, *Annalen der Physik* **505**, 535 (1993).
  - [27] A. J. Leggett, On the Superfluid Fraction of an Arbitrary Many-Body System at T=0, *Journal of Statistical Physics* **93**, 927 (1998).
  - [28] F. London and H. London, The electromagnetic equations of the superconductor, *Proceedings of the Royal Society A* **149**, 71 (1935).
  - [29] D. N. Basov and A. V. Chubukov, Manifesto for a higher T<sub>c</sub>, *Nature Physics* **7**, 272 (2011).
  - [30] M. Tovmasyan, S. Peotta, P. Törmä, and S. D. Huber, Effective theory and emergent SU(2) symmetry in the flat bands of attractive Hubbard models, *Phys. Rev. B* **94**, 245149 (2016).
  - [31] E. Rossi, Quantum metric and correlated states in two-dimensional systems, *Current Opinion in Solid State and Materials Science* **25**, 100952 (2021).
  - [32] M. Iskin, Two-body problem in a multiband lattice and the role of quantum geometry, *Phys. Rev. A* **103**, 053311 (2021).



- (2021).
- [33] K. Moon, H. Mori, K. Yang, S. M. Girvin, A. H. MacDonald, L. Zheng, D. Yoshioka, and S.-C. Zhang, Spontaneous interlayer coherence in double-layer quantum Hall systems: Charged vortices and Kosterlitz-Thouless phase transitions, *Physical Review B* **51**, 5138 (1995).
  - [34] N. B. Kopnin, Surface superconductivity in multilayered rhombohedral graphene: Supercurrent, *JETP Letters* **94**, 81 (2011).
  - [35] N. Marzari, A. A. Mostofi, J. R. Yates, I. Souza, and D. Vanderbilt, Maximally localized Wannier functions: Theory and applications, *Rev. Mod. Phys.* **84**, 1419 (2012).
  - [36] C.-K. Chiu, J. C. Y. Teo, A. P. Schnyder, and S. Ryu, Classification of topological quantum matter with symmetries, *Reviews of Modern Physics* **88**, 035005 (2016).
  - [37] C. Brouder, G. Panati, M. Calandra, C. Mourougane, and N. Marzari, Exponential localization of Wannier functions in insulators, *Phys. Rev. Lett.* **98**, 046402 (2007).
  - [38] G. Panati, Triviality of Bloch and Bloch-Dirac Bundles, *Annales Henri Poincaré* **8**, 995 (2007).
  - [39] D. Monaco, G. Panati, A. Pisante, and S. Teufel, Optimal Decay of Wannier functions in Chern and Quantum Hall Insulators, *Communications in Mathematical Physics* **359**, 61 (2018).
  - [40] F. Xie, Z. Song, B. Lian, and B. A. Bernevig, Topology-bounded superfluid weight in twisted bilayer graphene, *Phys. Rev. Lett.* **124**, 167002 (2020).
  - [41] J. Herzog-Arbeitman, V. Peri, F. Schindler, S. D. Huber, and B. A. Bernevig, Superfluid weight bounds from symmetry and quantum geometry in flat bands, *arXiv:2110.14663* (2021).
  - [42] D. R. Nelson and J. M. Kosterlitz, Universal Jump in the Superfluid Density of Two-Dimensional Superfluids, *Physical Review Letters* **39**, 1201 (1977).
  - [43] J. S. Hofmann, E. Berg, and D. Chowdhury, Superconductivity, pseudogap, and phase separation in topological flat bands, *Phys. Rev. B* **102**, 201112 (2020).
  - [44] V. Peri, Z.-D. Song, B. A. Bernevig, and S. D. Huber, Fragile topology and flat-band superconductivity in the strong-coupling regime, *Phys. Rev. Lett.* **126**, 027002 (2021).
  - [45] M. Tovmasyan, S. Peotta, L. Liang, P. Törmä, and S. D. Huber, Preformed pairs in flat Bloch bands, *Phys. Rev. B* **98**, 134513 (2018).
  - [46] R. Mondaini, G. G. Batrouni, and B. Grémaud, Pairing and superconductivity in the flat band: Creutz lattice, *Physical Review B* **98**, 155142 (2018).
  - [47] S. M. Chan, B. Grémaud, and G. G. Batrouni, Pairing and superconductivity in quasi one-dimensional flat band systems: Creutz and sawtooth lattices, *arXiv:2105.12761 [cond-mat]* (2021), *arXiv:2105.12761 [cond-mat]*.
  - [48] R. Bistritzer and A. H. MacDonald, Moiré bands in twisted double-layer graphene, *Proceedings of the National Academy of Sciences* **108**, 12233 (2011).
  - [49] Y. Cao, V. Fatemi, A. Demir, S. Fang, S. L. Tomarken, J. Y. Luo, J. D. Sanchez-Yamagishi, K. Watanabe, T. Taniguchi, E. Kaxiras, R. C. Ashoori, and P. Jarillo-Herrero, Correlated insulator behaviour at half-filling in magic-angle graphene superlattices, *Nature* **556**, 80 (2018).
  - [50] Y. Cao, V. Fatemi, S. Fang, K. Watanabe, T. Taniguchi, E. Kaxiras, and P. Jarillo-Herrero, Unconventional superconductivity in magic-angle graphene superlattices, *Nature* **556**, 43 (2018).
  - [51] X. Lu, P. Stepanov, W. Yang, M. Xie, M. A. Aamir, I. Das, C. Urgell, K. Watanabe, T. Taniguchi, G. Zhang, A. Bachtold, A. H. MacDonald, and D. K. Efetov, Superconductors, orbital magnets and correlated states in magic-angle bilayer graphene, *Nature* **574**, 653 (2019).
  - [52] M. Yankowitz, S. Chen, H. Polshyn, Y. Zhang, K. Watanabe, T. Taniguchi, D. Graf, A. F. Young, and C. R. Dean, Tuning superconductivity in twisted bilayer graphene, *Science* **363**, 1059 (2019).
  - [53] Y. Saito, J. Ge, K. Watanabe, T. Taniguchi, and A. F. Young, Independent superconductors and correlated insulators in twisted bilayer graphene, *Nature Physics* **16**, 926–930 (2020).
  - [54] P. Stepanov, I. Das, X. Lu, A. Fahimniya, K. Watanabe, T. Taniguchi, F. H. L. Koppens, J. Lischner, L. Levitov, and D. K. Efetov, Untying the insulating and superconducting orders in magic-angle graphene, *Nature* **583**, 375–378 (2020).
  - [55] X. Liu, Z. Wang, K. Watanabe, T. Taniguchi, O. Vafek, and J. Li, Tuning electron correlation in magic-angle twisted bilayer graphene using Coulomb screening, *Science* **371**, 1261 (2021).
  - [56] M. Serlin, C. L. Tschirhart, H. Polshyn, Y. Zhang, J. Zhu, K. Watanabe, T. Taniguchi, L. Balents, and A. F. Young, Intrinsic quantized anomalous Hall effect in a moiré heterostructure, *Science* **367**, 900–903 (2019).
  - [57] Y. Xie, B. Lian, B. Jäck, X. Liu, C.-L. Chiu, K. Watanabe, T. Taniguchi, B. A. Bernevig, and A. Yazdani, Spectroscopic signatures of many-body correlations in magic-angle twisted bilayer graphene, *Nature* **572**, 101 (2019).
  - [58] Y. Choi, J. Kemmer, Y. Peng, A. Thomson, H. Arora, R. Polski, Y. Zhang, H. Ren, J. Alicea, G. Refael, F. von Oppen, K. Watanabe, T. Taniguchi, and S. Nadj-Perge, Electronic correlations in twisted bilayer graphene near the magic angle, *Nature Physics* **15**, 1174–1180 (2019).
  - [59] K. P. Nuckolls, M. Oh, D. Wong, B. Lian, K. Watanabe, T. Taniguchi, B. A. Bernevig, and A. Yazdani, Strongly correlated Chern insulators in magic-angle twisted bilayer graphene, *Nature* **588**, 610 (2020).
  - [60] Y. Choi, H. Kim, Y. Peng, A. Thomson, C. Lewandowski, R. Polski, Y. Zhang, H. S. Arora, K. Watanabe, T. Taniguchi, J. Alicea, and S. Nadj-Perge, Correlation-driven topological phases in magic-angle twisted bilayer graphene, *Nature* **589**, 536 (2021).
  - [61] I. Das, X. Lu, J. Herzog-Arbeitman, Z.-D. Song, K. Watanabe, T. Taniguchi, B. A. Bernevig, and D. K. Efetov, Symmetry broken Chern insulators and magic series of Rashba-like Landau level crossings in magic angle bilayer graphene, *Nat. Phys.* **17**, 710 (2021).
  - [62] S. Wu, Z. Zhang, K. Watanabe, T. Taniguchi, and E. Y. Andrei, Chern insulators, van Hove singularities and topological flat bands in magic-angle twisted bilayer graphene, *Nature Materials* **20**, 488 (2021).
  - [63] X. Lu, B. Lian, G. Chaudhary, B. A. Piot, G. Romagnoli, K. Watanabe, T. Taniguchi, M. Poggio, A. H. MacDonald, B. A. Bernevig, and D. K. Efetov, Multiple flat bands and topological Hofstadter butterfly in twisted bilayer graphene close to the second magic angle, *Proceedings of the National Academy of Sciences* **118**, e2100006118 (2021).



- [64] G. W. Burg, B. Lian, T. Taniguchi, K. Watanabe, B. A. Bernevig, and E. Tutuc, Evidence of emergent symmetry and valley Chern number in twisted double-bilayer graphene (2020), [arXiv:2006.14000 \[cond-mat.mes-hall\]](#).
- [65] L. Zou, H. C. Po, A. Vishwanath, and T. Senthil, Band structure of twisted bilayer graphene: Emergent symmetries, commensurate approximants, and Wannier obstructions, *Phys. Rev. B* **98**, 085435 (2018).
- [66] Y. Fu, E. J. König, J. H. Wilson, Y.-Z. Chou, and J. H. Pixley, Magic-angle semimetals, *npj Quantum Materials* **5**, 71 (2020).
- [67] J. Liu, J. Liu, and X. Dai, Pseudo Landau level representation of twisted bilayer graphene: Band topology and implications on the correlated insulating phase, *Physical Review B* **99**, 155415 (2019).
- [68] J. Kang and O. Vafek, Symmetry, Maximally Localized Wannier States, and a Low-Energy Model for Twisted Bilayer Graphene Narrow Bands, *Phys. Rev. X* **8**, 031088 (2018).
- [69] Z. Song, Z. Wang, W. Shi, G. Li, C. Fang, and B. A. Bernevig, All Magic Angles in Twisted Bilayer Graphene are Topological, *Physical Review Letters* **123**, 036401 (2019).
- [70] H. C. Po, L. Zou, T. Senthil, and A. Vishwanath, Faithful tight-binding models and fragile topology of magic-angle bilayer graphene, *Physical Review B* **99**, 195455 (2019).
- [71] J. Ahn, S. Park, and B.-J. Yang, Failure of Nielsen-Ninomiya Theorem and Fragile Topology in Two-Dimensional Systems with Space-Time Inversion Symmetry: Application to Twisted Bilayer Graphene at Magic Angle, *Physical Review X* **9**, 021013 (2019).
- [72] A. Bouhon, A. M. Black-Schaffer, and R.-J. Slager, Wilson loop approach to fragile topology of split elementary band representations and topological crystalline insulators with time-reversal symmetry, *Phys. Rev. B* **100**, 195135 (2019).
- [73] B. Lian, F. Xie, and B. A. Bernevig, Landau level of fragile topology, *Phys. Rev. B* **102**, 041402 (2020).
- [74] K. Hejazi, C. Liu, and L. Balents, Landau levels in twisted bilayer graphene and semiclassical orbits, *Physical Review B* **100** (2019).
- [75] J. Kang and O. Vafek, Strong Coupling Phases of Partially Filled Twisted Bilayer Graphene Narrow Bands, *Physical Review Letters* **122**, 246401 (2019).
- [76] N. Bultinck, E. Khalaf, S. Liu, S. Chatterjee, A. Vishwanath, and M. P. Zaletel, Ground state and hidden symmetry of magic-angle graphene at even integer filling, *Phys. Rev. X* **10**, 031034 (2020).
- [77] H. C. Po, L. Zou, A. Vishwanath, and T. Senthil, Origin of Mott Insulating Behavior and Superconductivity in Twisted Bilayer Graphene, *Physical Review X* **8**, 031089 (2018).
- [78] A. Julku, T. Peltonen, L. Liang, T. Heikkilä, and P. Törmä, Superfluid weight and Berezinskii-Kosterlitz-Thouless transition temperature of twisted bilayer graphene, *Phys. Rev. B* **101**, 060505 (2020).
- [79] X. Hu, T. Hyart, D. I. Pikulin, and E. Rossi, Geometric and conventional contribution to the superfluid weight in twisted bilayer graphene, *Phys. Rev. Lett.* **123**, 237002 (2019).
- [80] J. Kang and O. Vafek, Non-abelian dirac node braiding and near-degeneracy of correlated phases at odd integer filling in magic-angle twisted bilayer graphene, *Phys. Rev. B* **102**, 035161 (2020).
- [81] T. Soejima, D. E. Parker, N. Bultinck, J. Hauschild, and M. P. Zaletel, Efficient simulation of moiré materials using the density matrix renormalization group, *Phys. Rev. B* **102**, 205111 (2020).
- [82] J. H. Pixley and E. Y. Andrei, Ferromagnetism in magic-angle graphene, *Science* **365**, 543 (2019).
- [83] M. Xie and A. H. MacDonald, Nature of the correlated insulator states in twisted bilayer graphene, *Phys. Rev. Lett.* **124**, 097601 (2020).
- [84] J. Liu and X. Dai, Theories for the correlated insulating states and quantum anomalous Hall effect phenomena in twisted bilayer graphene, *Phys. Rev. B* **103**, 035427 (2021).
- [85] T. Cea and F. Guinea, Band structure and insulating states driven by Coulomb interaction in twisted bilayer graphene, *Phys. Rev. B* **102**, 045107 (2020).
- [86] Y. Da Liao, J. Kang, C. N. Breið, X. Y. Xu, H.-Q. Wu, B. M. Andersen, R. M. Fernandes, and Z. Y. Meng, Correlation-induced insulating topological phases at charge neutrality in twisted bilayer graphene, *Phys. Rev. X* **11**, 011014 (2021).
- [87] A. Abouelkomsan, Z. Liu, and E. J. Bergholtz, Particle-hole duality, emergent Fermi liquids, and fractional Chern insulators in moiré flatbands, *Phys. Rev. Lett.* **124**, 106803 (2020).
- [88] C. Repellin and T. Senthil, Chern bands of twisted bilayer graphene: Fractional Chern insulators and spin phase transition, *Phys. Rev. Research* **2**, 023238 (2020).
- [89] O. Vafek and J. Kang, Renormalization group study of hidden symmetry in twisted bilayer graphene with coulomb interactions, *Phys. Rev. Lett.* **125**, 257602 (2020).
- [90] R. M. Fernandes and J. W. F. Venderbos, Nematicity with a twist: Rotational symmetry breaking in a moiré superlattice, *Science Advances* **6** (2020).
- [91] J. H. Wilson, Y. Fu, S. Das Sarma, and J. H. Pixley, Disorder in twisted bilayer graphene, *Phys. Rev. Research* **2**, 023325 (2020).
- [92] J. Wang, Y. Zheng, A. J. Millis, and J. Cano, Chiral approximation to twisted bilayer graphene: Exact intravalley inversion symmetry, nodal structure, and implications for higher magic angles, *Phys. Rev. Research* **3**, 023155 (2021).
- [93] Z.-D. Song, B. Lian, N. Regnault, and B. A. Bernevig, Twisted bilayer graphene. II. stable symmetry anomaly, *Phys. Rev. B* **103**, 205412 (2021).
- [94] B. A. Bernevig, B. Lian, A. Cowsik, F. Xie, N. Regnault, and Z.-D. Song, Twisted bilayer graphene. V. exact analytic many-body excitations in Coulomb hamiltonians: Charge gap, Goldstone modes, and absence of Cooper pairing, *Phys. Rev. B* **103**, 205415 (2021).
- [95] B. Lian, Z.-D. Song, N. Regnault, D. K. Efetov, A. Yazdani, and B. A. Bernevig, Twisted bilayer graphene. IV. exact insulator ground states and phase diagram, *Phys. Rev. B* **103**, 205414 (2021).
- [96] X. Zhang, K.-T. Tsai, Z. Zhu, W. Ren, Y. Luo, S. Carr, M. Lusk, E. Kaxiras, and K. Wang, Correlated insulating states and transport signature of superconductivity in twisted trilayer graphene superlattices, *Phys. Rev. Lett.* **127**, 166802 (2021).
- [97] G. Chen, A. L. Sharpe, P. Gallagher, I. T. Rosen, E. J. Fox, L. Jiang, B. Lyu, H. Li, K. Watanabe, T. Taniguchi, J. Jung, Z. Shi, D. Goldhaber-Gordon, Y. Zhang, and F. Wang, Signatures of tunable superconductivity in a

- trilayer graphene moiré superlattice, *Nature* **572**, 215 (2019).
- [98] J. Park, Y. Cao, K. Watanabe, T. Taniguchi, and P. Jarillo-Herrero, Tunable strongly coupled superconductivity in magic-angle twisted trilayer graphene, *Nature* **590**, 249 (2021).
  - [99] L. Classen, Geometry rescues superconductivity in twisted graphene, *Physics* **13**, 23 (2020).
  - [100] Y. Su and S.-Z. Lin, Pairing symmetry and spontaneous vortex-antivortex lattice in superconducting twisted-bilayer graphene: Bogoliubov-de Gennes approach, *Phys. Rev. B* **98**, 195101 (2018).
  - [101] J. M. B. Lopes dos Santos, N. M. R. Peres, and A. H. Castro Neto, Graphene bilayer with a twist: Electronic structure, *Phys. Rev. Lett.* **99**, 256802 (2007).
  - [102] Z. Wang, G. Chaudhary, Q. Chen, and K. Levin, Quantum geometric contributions to the BKT transition: Beyond mean field theory, *Phys. Rev. B* **102**, 184504 (2020).
  - [103] T. Kitamura, T. Yamashita, J. Ishizuka, A. Daido, and Y. Yanase, Superconductivity in monolayer FeSe enhanced by quantum geometry, [arXiv:2108.10002 \[cond-mat\]](#) (2021), [arXiv:2108.10002 \[cond-mat\]](#).
  - [104] D.-H. Lee, Hunting down unconventional superconductors, *Science* **357**, 32 (2017).
  - [105] S. V. Gallego, E. S. Tasci, G. Flor, J. M. Perez-Mato, and M. I. Aroyo, Magnetic symmetry in the Bilbao crystallographic server: a computer program to provide systematic absences of magnetic neutron diffraction, *Journal of Applied Crystallography* **45**, 1236 (2012).
  - [106] A. Alexandradinata, X. Dai, and B. A. Bernevig, Wilson-loop characterization of inversion-symmetric topological insulators, *Phys. Rev. B* **89**, 155114 (2014).
  - [107] J. Ahn, D. Kim, Y. Kim, and B.-J. Yang, Band Topology and Linking Structure of Nodal Line Semimetals with  $\mathbb{Z}_2$  Monopole Charges, *Physical Review Letters* **121**, 106403 (2018).
  - [108] F. N. Ünal, A. Bouhon, and R.-J. Slager, Topological euler class as a dynamical observable in optical lattices, *Phys. Rev. Lett.* **125**, 053601 (2020).
  - [109] H. C. Po, H. Watanabe, and A. Vishwanath, Fragile Topology and Wannier Obstructions, *Physical Review Letters* **121**, 126402 (2018).
  - [110] J. Cano, B. Bradlyn, Z. Wang, L. Elcoro, M. G. Vergniory, C. Felser, M. I. Aroyo, and B. A. Bernevig, Topology of disconnected elementary band representations, *Phys. Rev. Lett.* **120**, 266401 (2018).
  - [111] R. Yu, X. L. Qi, A. Bernevig, Z. Fang, and X. Dai, Equivalent expression of  $\mathbb{Z}_2$  topological invariant for band insulators using the non-Abelian Berry connection, *Phys. Rev. B* **84**, 075119 (2011).
  - [112] N. Bultinck, S. Chatterjee, and M. P. Zaletel, Mechanism for anomalous hall ferromagnetism in twisted bilayer graphene, *Phys. Rev. Lett.* **124**, 166601 (2020).
  - [113] B. A. Bernevig, Z.-D. Song, N. Regnault, and B. Lian, Twisted bilayer graphene. III. interacting Hamiltonian and exact symmetries, *Phys. Rev. B* **103**, 205413 (2021).
  - [114] Z. Meng, L. Wang, W. Han, F. Liu, K. Wen, C. Gao, P. Wang, C. Chin, and J. Zhang, Atomic Bose-Einstein condensate in a twisted-bilayer optical lattice, [arXiv:2110.00149 \[cond-mat\]](#) (2021), [arXiv:2110.00149 \[cond-mat\]](#).
  - [115] I. Bloch, J. Dalibard, and W. Zwerger, Many-body physics with ultracold gases, *Reviews of Modern Physics* **80**, 885 (2008).
  - [116] S. Giorgini, L. P. Pitaevskii, and S. Stringari, Theory of ultracold atomic Fermi gases, *Reviews of Modern Physics* **80**, 1215 (2008).
  - [117] P. Törmä and K. Sengstock, eds., *Quantum Gas Experiments: Exploring Many-Body States*, Cold Atoms No. vol. 3 (Imperial College Press, London, 2015).
  - [118] M. Lewenstein, A. Sanpera, and V. Ahufinger, *Ultracold Atoms in Optical Lattices: Simulating Quantum Many-Body Systems*, 1st ed. (Oxford University Press, Oxford, U.K, 2012).
  - [119] P. Soltan-Panahi, J. Struck, P. Hauke, A. Bick, W. Plenkers, G. Meineke, C. Becker, P. Windpassinger, M. Lewenstein, and K. Sengstock, Multi-component quantum gases in spin-dependent hexagonal lattices, *Nature Physics* **7**, 434 (2011).
  - [120] L. Tarruell, D. Greif, T. Uehlinger, G. Jotzu, and T. Esslinger, Creating, moving and merging Dirac points with a Fermi gas in a tunable honeycomb lattice, *Nature* **483**, 302 (2012).
  - [121] G.-B. Jo, J. Guzman, C. K. Thomas, P. Hosur, A. Vishwanath, and D. M. Stamper-Kurn, Ultracold atoms in a tunable optical kagome lattices, *Phys. Rev. Lett.* **108**, 045305 (2012).
  - [122] S. Taie, H. Ozawa, T. Ichinose, T. Nishio, S. Nakajima, and Y. Takahashi, Coherent driving and freezing of bosonic matter wave in an optical Lieb lattice, *Sci. Adv.* **1**, 10 (2015).
  - [123] M. Mancini, G. Pagano, G. Cappellini, L. Livi, M. Rider, J. Catani, C. Sias, P. Zoller, M. Inguscio, M. Dalmonte, and L. Fallani, Observation of chiral edge states with neutral fermions in synthetic Hall ribbons, *Science* **349**, 1510 (2015).
  - [124] B. K. Stuhl, H.-I. Lu, L. M. Ayccock, D. Genkina, and I. B. Spielman, Visualizing edge states with an atomic Bose gas in the quantum Hall regime, *Science* **349**, 1514 (2015).
  - [125] T. Ozawa and H. M. Price, Topological quantum matter in synthetic dimensions, *Nature Reviews Physics* **1**, 349 (2019).
  - [126] A. González-Tudela and J. I. Cirac, Cold atoms in twisted-bilayer optical potentials, *Physical Review A* **100**, 053604 (2019).
  - [127] T. Salamon, A. Celi, R. W. Chhajlany, I. Frérot, M. Lewenstein, L. Tarruell, and D. Rakshit, Simulating twistronics without a twist, *Phys. Rev. Lett.* **125**, 030504 (2020).
  - [128] T. Salamon, R. W. Chhajlany, A. Dauphin, M. Lewenstein, and D. Rakshit, Quantum anomalous Hall phase in synthetic bilayers via twistronics without a twist, *Physical Review B* **102**, 235126 (2020).
  - [129] I. Carusotto and Y. Castin, Nonequilibrium and local detection of the normal fraction of a trapped two-dimensional Bose gas, *Physical Review A* **84**, 053637 (2011).
  - [130] L. A. Sidorenkov, M. K. Tey, R. Grimm, Y.-H. Hou, L. Pitaevskii, and S. Stringari, Second sound and the superfluid fraction in a Fermi gas with resonant interactions, *Nature* **498**, 78 (2013).
  - [131] T.-L. Ho and Q. Zhou, Obtaining the phase diagram and thermodynamic quantities of bulk systems from the densities of trapped gases, *Nature Physics* **6**, 131 (2010).
  - [132] S. T. John, Z. Hadzibabic, and N. R. Cooper, Spectroscopic method to measure the superfluid fraction of an ultracold atomic gas, *Physical Review A* **83**, 023610 (2011).

- (2011).
- [133] J. M. Edge and N. R. Cooper, Probing ultracold Fermi gases with light-induced gauge potentials, *Physical Review A* **83**, 053619 (2011).
  - [134] S. Peotta, C.-C. Chien, and M. Di Ventra, Phase-induced transport in atomic gases: From superfluid to Mott insulator, *Physical Review A* **90**, 053615 (2014).
  - [135] D. Rossini, R. Fazio, V. Giovannetti, and A. Silva, Quantum quenches, linear response and superfluidity out of equilibrium, *EPL (Europhysics Letters)* **107**, 30002 (2014).
  - [136] S. Krinner, T. Esslinger, and J.-P. Brantut, Two-terminal transport measurements with cold atoms, *J. Phys. Cond. Mat.* **29**, 343003 (2017).
  - [137] S. Krinner, D. Stadler, D. Husmann, J.-P. Brantut, and T. Esslinger, Observation of quantized conductance in neutral matter, *Nature* **517**, 14049 (2015).
  - [138] S. Krinner, D. Stadler, J. Meineke, J.-P. Brantut, and T. Esslinger, Superfluidity with disorder in a thin film of quantum gas, *Physical Review Letters* **110**, 100601 (2013).
  - [139] V. A. J. Pyykkönen, S. Peotta, P. Fabritius, J. Mohan, T. Esslinger, and P. Törmä, Flat-band transport and Josephson effect through a finite-size sawtooth lattice, *Physical Review B* **103**, 144519 (2021).
  - [140] K.-E. Huhtinen and P. Törmä, Possible insulator-pseudogap crossover in the attractive Hubbard model on the lieb lattice, *Phys. Rev. B* **103**, L220502 (2021).
  - [141] A. Mazurenko, C. S. Chiu, G. Ji, M. F. Parsons, M. Kanász-Nagy, R. Schmidt, F. Grusdt, E. Demler, D. Greif, and M. Greiner, A cold-atom Fermi-Hubbard antiferromagnet, *Nature* **545**, 462 (2017).
  - [142] P. E. Dolgirev, S. Chatterjee, I. Esterlis, A. A. Zibrov, M. D. Lukin, N. Yao, and E. Demler, Characterizing two-dimensional superconductivity via nanoscale noise magnetometry with single-spin qubits, (2021), [arXiv:2106.05283](#).
  - [143] Y. Jia, P. Wang, C.-L. Chiu, Z. Song, G. Yu, B. Jäck, S. Lei, S. Klemen, F. A. Cevallos, M. Onyszczyk, N. Fishchenko, X. Liu, G. Farahi, F. Xie, Y. Xu, K. Watanabe, T. Taniguchi, B. A. Bernevig, R. J. Cava, L. M. Schoop, A. Yazdani, and S. Wu, Evidence for a monolayer excitonic insulator, (2020), [arXiv:2010.05390 \[cond-mat.mes-hall\]](#).
  - [144] P. Wang, G. Yu, Y. H. Kwan, Y. Jia, S. Lei, S. Klemen, F. A. Cevallos, T. Devakul, K. Watanabe, T. Taniguchi, S. L. Sondhi, R. J. Cava, L. M. Schoop, S. A. Parameswaran, and S. Wu, One-dimensional Luttinger liquids in a two-dimensional moiré lattice, (2021), [arXiv:2109.04637 \[cond-mat.mes-hall\]](#).
  - [145] H. Zhou, T. Xie, T. Taniguchi, K. Watanabe, and A. F. Young, Superconductivity in rhombohedral trilayer graphene (2021), [arXiv:2106.07640 \[cond-mat.mes-hall\]](#).
  - [146] J. S. Hofmann, D. Chowdhury, S. A. Kivelson, and E. Berg, Superconductivity is boundless, (2021), [arXiv:2105.09322](#).
  - [147] T. Hazra, N. Verma, and M. Randeria, Bounds on the Superconducting Transition Temperature: Applications to Twisted Bilayer Graphene and Cold Atoms, *Physical Review X* **9**, 031049 (2019).
  - [148] G. E. Topp, C. J. Eckhardt, D. M. Kennes, M. A. Sentef, and P. Törmä, Light-matter coupling and quantum geometry in moiré materials, *Phys. Rev. B* **104**, 064306 (2021).
  - [149] S. Chaudhary, G. Lewandowski, and G. Refael, Shift-current response as a probe of quantum geometry and electron-electron interactions in twisted bilayer graphene, (2021), [arXiv:2107.09090](#).
  - [150] A. Julku, G. M. Bruun, and P. Törmä, Quantum geometry and flat band Bose-Einstein condensation, *Phys. Rev. Lett.* **127**, 170404 (2021).